1

2

Regulation of the macrolide resistance ABC-F translation factor MsrD

4

5

Corentin R. Fostier[1], Farès Ousalem[1], Elodie C. Leroy[2], Saravuth Ngo[1],

Heddy Soufari[2,3], C. Axel Innis[2], Yaser Hashem[2,*], Grégory Boël[1,4,*]

8

[1]Expression Génétique Microbienne, CNRS, Université Paris Cité, Institut de Biologie Physico-Chimique, 75005 Paris, France

[2]INSERM U1212 (ARNA), Institut Européen de Chimie et Biologie, Université de Bordeaux, 33607 Pessac, France

[3]Current address: NovAliX, Boulevard Sébastien Brant, Bioparc, 67405 Illkirch Cedex, France

[4]Lead contact

*Correspondence:

Grégory Boël, Institut de Biologie Physico-Chimique, 13 rue Pierre et Marie Curie, 75005 Paris, France, tel. : +33 (0) 1 58 41 51 21; e-mail: boel@ibpc.fr

Yaser Hashem, Institut Européen de Chimie et Biologie, Université de Bordeaux, 33607 Pessac, France, tel. : +33 (0) 5 40 00 88 22; e-mail: yaser.hashem@inserm.fr

20

1

SUMMARY

Antibiotic resistance ABC-Fs (ARE ABC-Fs) are translation factors currently proliferating among human pathogens that provide resistance against clinically important ribosome-targeting antibiotics. Here, we combine genetic and structural approaches to determine the regulation of *streptococcal* ARE ABC-F gene *msrD* in response to macrolide exposure and also demonstrate that MsrD twin-ATPase sites work asymmetrically to mediate the dynamic of MsrD interaction with the ribosome. We show that cladinose-containing macrolides lead to insertion of MsrDL leader peptide into an undocumented conserved crevice of the ribosomal exit tunnel concomitantly with 23S rRNA rearrangements that prevent peptide bond formation and preclude accommodation of release factors. The stalled ribosome obstructs formation of a Rho-independent terminator which prevents *msrD* transcriptional attenuation. This stalled ribosome is rescued by MsrD, but not by MsrD mutants which do not provide antibiotic resistance, showing evidence of equivalence between MsrD function in antibiotic resistance and its action on this complex.

KEYWORDS

Ribosome, protein synthesis, antibiotic resistance, ARE ABC-F protein family, leader peptide, cryo-EM.

INTRODUCTION

ABC-F ATPases belonging to the ATP-Binding Cassette (ABC) superfamily are translation factors and some of them, termed antibiotic resistance ABC-Fs (ARE ABC-Fs), confer resistance to clinically important antibiotics that bind to the ribosomal peptidyl transferase center (PTC) and/or the nascent peptide exit tunnel (NPET)[1–7]. ABC-F proteins are composed of two ABC domains (or Nucleotide Binding Domains, NBDs) joined by a linker region called P-site tRNA-interaction motif (PtIM)[8,9], also termed antibiotic resistance determinant (ARD) for ARE ABC-Fs[1–3]. The two ABC domains dimerize after binding of two ATP molecules and in this conformation the factor can bind the ribosomal E-site[9], where the PtIM adopts an α-helical hairpin conformation that interacts directly with the peptidyl-tRNA and extends toward the PTC/NPET. Three antibiotic resistance phenotypes are associated with ARE ABC-Fs: (i) MKS$_B$ (Macrolides, Ketolides, Streptogramins group B); (ii) PLS$_A$ (Pleuromutilins, Lincosamides, Streptogramins group A); (iii) PhO (Phenicols, Oxazolidinones)[10,11]. However, despite structural investigations[1–3,5,7], the exact molecular mechanism of action of ARE ABC-Fs remains unclear.

Over the last forty years, biochemical and structural investigations demonstrated the ability of elongating nascent chains (NC) into the ribosomal tunnel to interact with metabolites or antibiotics, thus adapting protein synthesis to environmental cues[12–16]. In human pathogens, antibiotic-dependent formation of stalled ribosome complexes (SRCs) on regulatory ORFs, named leader peptides, can subsequently allow regulation of downstream resistance genes in response to antibiotic exposure[17–20].

ARE ABC-F gene *msrD* is a member of the *msr* (macrolide and streptogramin B resistant) gene group previously referred as *mel*[21,22]. This gene is generally found in operon with a macrolide efflux facilitator (*mefA* or *mefE) gene*, the two corresponding proteins acting synergistically to confer macrolide resistance[23–26]. This operon is part of the Macrolide Efflux Genetic Assembly (MEGA)[27,28] that disseminates in human pathogens on mobile genetic elements: conjugative transposons like the tn916-type[29] and conjugative prophages like the Φ1207.3[30] among *Streptococci*, conjugative plasmids like the pMUR050 [31] among

3

67 *Enterobacteria*. In *Streptococci*, the operon is transcribed in presence of erythromycin (ERY)

68 as a polycistronic mRNA from a single promoter located ~350 bp upstream *mefA*[32,33]. It is also

69 regulated by ribosome-mediated transcription attenuation via MefAL leader peptide

70 (MTASMRLR), which is closely related to ErmDL leader peptide (MTHSMRLRFPTLNQ), both

71 polypeptides harboring the characteristic macrolide-arrest motif Arg/Lys-X-Arg/Lys so called

72 "+x+"[14,33–35].

73   Here, we report the presence of a second transcriptional attenuator on the *mefA/msrD*

74 operon regulating exclusively *msrD* expression upon macrolide exposure. Presence of ERY

75 induces ribosome stalling on the previously identified *msrDL* leader peptide (encoding

76 MYLIFM)[34], allowing RNA polymerase (RNAP) to bypass an intrinsic terminator. Our findings

77 demonstrate stalling occurs due to hampered translation termination on UAA stop codon,

78 action of both release factors 1 and 2 (RF1 and RF2) being inhibited. Our results are supported

79 by the cryo-EM structure of MsrDL-SRC that provides molecular insight on how the PTC

80 precludes productive accommodation of RF1/RF2 and how the NC discriminates tunnel-bound

81 cladinose-containing macrolides. The path of the NC within the tunnel greatly differs from

82 previously described leader peptides[12–16] with the NC latching into a ribosomal crevice,

83 conserved from prokaryotes to eukaryotes, delimited by 23S rRNA nucleotides U2584, U2586,

84 G2608 and C2610 that may form a novel ribosomal functional site. Finally, our results

85 demonstrate that the two ATPase sites of MsrD perform different functions and the protein can

86 negatively self-regulate its synthesis in presence of ERY by direct action on MsrDL-stalled

87 ribosomes.

88

89 **RESULTS**

90 **MsrD provides macrolide and ketolide resistance by direct interaction with ribosome**

91   The *mefA/msrD* macrolide resistance operon (Fig. 1a) is part of the MEGA element

92 currently spreading among clinical isolates and livestock[33,36–38]. A phylogenetic analysis

93 (Supplementary fig. 1a) shows that the operon disseminates predominantly in Gram-positive

94 firmicutes (mostly *Streptococci*) and in some Gram-negative proteobacteria (such as

4

95   *Haemophilus influenzae, Neisseria gonorrhoeae or Escherichia coli*). Gene *msrD* shares ~62

96   % identity with its closest homolog *msrE*[7], both factors exhibiting the canonical ABC-F

97   organization (Fig. 1b and Supplementary fig. 1b).

98   Model bacteria *Escherichia coli* (*E. coli*) presents undeniable advantages for genetic

99   and molecular biology, but presence of multidrug efflux systems greatly limits its use in

100   antibiotic research[39,40]. To circumvent this limitation, we took advantage of *E. coli* DB10 strain

101   which exhibits exacerbated sensitivity toward macrolide antibiotics[41]. Heterologous expression

102   of $msrD_{WT}$ from an arabinose-inducible promoter conferred macrolide and ketolide resistance

103   phenotype to *E. coli* DB10 strain (Table 1), demonstrating the functionality of the factor in this

104   organism. Expression of $msrD_{WT}$ resulted in 8-fold m̲inimal i̲nhibitory c̲oncentration (MIC)

105   increase for 14-membered macrolide ERY, 8-fold for 15-membered macrolide azithromycin

106   (AZI) and 2-fold for telithromycin (TEL, ketolide antibiotic derived from 14-membered

107   macrolides). Similar results were reported for *Streptococcus pneumoniae* clinical isolates[23].

108   However, no change in MIC was observed for 16-membered macrolides tylosin (TYL) and

109   spiramycin (SPI), neither for non-macrolide antibiotics lincomycin (LNC), linezolid (LNZ) and

110   retapamulin (RTP) (Table 1).

111   Comparison of polysome profiles from bacteria unexposed or exposed to ERY show a

112   stabilization of ribosome disomes (Fig. 1c, 1d and Supplementary fig. 1c) as expected for an

113   antibiotic that inhibits ribosome elongation. The disome accumulation likely results from

114   elongating ribosomes that collide on ERY-stalled ribosomes arrested at the beginning of the

115   coding sequence. In presence of ERY ribosomes preferentially stall when they encounter "+x+"

116   motifs which are present in the first 30 amino-acids of ~25% of *E. coli* proteins[42,43]. Expression

117   of $msrD_{WT}$ alleviates the accumulation of disomes and restores a profile identical to that without

118   ERY (Fig. 1d versus 1c and Supplementary fig. 1c). Western blots of the polysome fractions

119   show an $MsrD_{WT}$ association with the 70S ribosome and the 50S subunit and polysomes (Fig.

120   1d and Supplementary fig. 1c). These results agree with a model in which $MsrD_{WT}$ directly

121   rescues ERY-stalled ribosomes and that MsrD can restore normal translation in presence of

122   the antibiotic.

5

123   To understand the function of the ATPase activity of MsrD, we constructed ATPase-

124   deficient variants $MsrD_{E125Q}$, $MsrD_{E434Q}$ and $MsrD_{E125Q/E434Q}$ (hereafter referred as $MsrD_{EQ2}$) by

125   replacing the catalytic glutamic acid residue (E) in Walker B motif of each or both ABC domain

126   by a glutamine (Q) (Fig. 1b and Supplementary fig. 1b). This mutation strongly reduces the

127   ATP hydrolysis while preserving the local stereochemistry of active site and has been

128   extensively used to trap ABC-F factors on the ribosome in ATP-bound conformation[1–3,5,9].

129   Expression of $msrD_{EQ2}$ in absence of ERY inhibits cell growth after $OD_{600}=0.4$ and shows an

130   accumulation of disomes on polysome profile (Supplementary fig. 1c) and western-blotting

131   reveals its association with the 30S subunit, 70S ribosome and polyribosomes (Fig. 1d and

132   Supplementary fig. 1c). These results shows that $MsrD_{EQ2}$ binds to the ribosome and inhibits

133   its elongation as observed for most of the ABC-F carrying the E-to-Q mutation[8,44]. In presence

134   of ERY, the disome and trisome accumulation increases and western blots show an increase

135   of $MsrD_{EQ2}$ in the disome fraction (Fig. 1d and Supplementary fig. 1c). Still, the ATPase activity

136   of MsrD impacts its binding preferences, $MsrD_{WT}$ interacting more with the 50S subunit in

137   contrast to $MsrD_{EQ2}$ interacting more with the 70S ribosome (Fig. 1d and Supplementary fig.

138   1c). Interestingly, the $MsrD_{E125Q}$ variant has an interaction profile with the ribosome similar to

139    $MsrD_{WT}$ whether $MsrD_{E434Q}$ has one closer to $MsrD_{EQ2}$.

140   A model consistent with these observations would imply that $MsrD_{WT}$ binds to ERY-

141   stalled ribosomes in an ATP-bound close conformation without the need of its ATPase activity,

142   then ATPase activity triggers 70S dissociation, $MsrD_{WT}$ staying associated with the 50S

143   subunit. Similar results were observed by expressing $msrD_{WT}$ and $msrD_{EQ2}$ in *E. coli* K12

144   MG1655 (Supplementary fig. 1d) in absence of ERY and with chloramphenicol being added to

145   stabilize polysomes. They also show a decrease of the 70S peak correlated with an increase

146   of 30S and 50S peaks for $msrD_{WT}$ condition when compared to the control, supporting the

147   proposed dissociation model. Western blots show more $MsrD_{EQ2}$ than $MsrD_{WT}$ in soluble

148   lysates (Supplementary fig. 1c) but $MsrD_{EQ2}$ inhibits protein synthesis including its own

149   synthesis. Therefore, we hypothesized that $MsrD_{EQ2}$ is less expressed but more soluble, which

150   has been confirmed with a solubility test (Supplementary fig. 1e).

151   We evaluated the influence of E-to-Q mutations of MsrD on bacterial growth and

152   antibiotic resistance phenotype. All the mutations impair bacterial growth and antibiotic

153   resistance phenotype (Fig. 1e), while $MsrD_{E125Q}$ and $MsrD_{EQ2}$ have a similar effect on bacterial

154   growth in absence or at low ERY concentration, $MsrD_{E434Q}$ is more toxic. However, $MsrD_{E125Q}$

155   variant maintains some resistance (MIC = 4 µM) compared to control (MIC = 2 µM) which is

156   also supported by the fact that $MsrD_{E125Q}$ IC_{50} is ~8 times higher than Control IC_{50} (Fig. 1e and

157   Supplementary Table 1). These results together with polysome profile experiments (Fig. 1c,

158   1d and Supplementary fig. 1d) suggest that interaction of MsrD with the 50S is necessary for

159   antibiotic resistance mechanism.

160   The two ATP hydrolysis sites (Supplementary fig. 1b) have therefore different tasks

161   and are functionally asymmetric, ATP site II achieving in part the mechanism of ERY-stalled

162   ribosome rescue. We also evaluated the importance of other residues of MsrD. Truncation of

163   the PtIM (replaced by three glycine) or just the Loop (ΔPtIM, ΔLoop respectively) completely

164   abolished the resistance phenotype *in vivo* (Fig. 1f) as reported *in vitro* for MsrE[7]. Punctual

165   mutations in the Loop (Fig. 1b) affect the resistance phenotype to a different extent, mutation

166   of R241 into alanine has almost no effect on the phenotype, but equivalent mutation for L242

167   or H244 reduces IC_{50} by ~3 fold (Fig. 1g and Supplementary Table 1), demonstrating that these

168   residues are important for MsrD function, but not essential even if they are predicted at the

169   vicinity of the antibiotic (Supplementary fig. 1f) in the MsrE-ribosome complex[7]. Interestingly,

170   this finding contrasts with mutagenesis assays for MsrE showing that mutation R241A reduces

171   the resistance by more than 50%. Replacement of H244 by the larger residue tryptophan

172   should displace the drug by steric occlusion, but the variant lost most of its antibiotic resistance

173   phenotype (Fig. 1g). Similarly, $MsrD_{WT}$ does not provide resistance to TYL nor SPI (Table 1),

174   while both antibiotics should clash with MsrD according to MsrE structure (Supplementary fig.

175   1f). Same observation can be made with LNC, LNZ or RTP (Table 1 and Supplementary fig.

176   1f). Therefore, MsrD action on the antibiotic is indirect and direct steric occlusion to displace

177   the antibiotic seems excluded.

178

Ribosome-mediated transcriptional attenuation regulates *msrD* expression

Analysis of the *mefA/msrD* operon sequence exposes a stringent ribosome binding site (RBS, whose sequence is 5'-GGAGGA-3') only 8 bp downstream *mefA* stop codon and possibly required for translation of the downstream putative small ORF *msrDL* (Supplementary fig. 2a). In order to test the influence of *msrDL* on *msrD* expression, a fluorescent reporter, which contains the sequence spanning from the first nucleotide downstream *mefA* stop codon to *msrD* three first codons fused to the Yellow Fluorescent Protein gene (YFP), was cloned in the low copy pMMB plasmid[45] under the control of IPTG-inducible $P_{LlacO-1}$ promoter[46]. The resulting plasmid, pMMB-*msrDL-msrD*$_{(1-3)}$:*yfp,* was used to directly follow the fluorescence reflecting *yfp* expression (Fig. 2a).

Basal fluorescence level was found stable in *E. coli* DB10 strain containing pMMB-*Control* independently of ERY concentration (Fig. 2a) while a fluorescence increase correlated with ERY concentration was observed in cells containing pMMB-*msrDL-msrD*$_{(1-3)}$:*yfp*, indicating an ERY-dependent induction. Optimal induction was found at 100 nM ERY while only 6.25 nM was sufficient to significantly induce *msrD*$_{(1-3)}$:*yfp* expression, demonstrating the high sensitivity of the system toward its inducer. A reduced, but significative fluorescence signal was detected at 0 nM ERY indicating an imperfect repression of the regulation . Inactivation of *msrDL* ORF by replacement of the start codon by an amber stop codon (pMMB-*msrDL*$_{(no\_ORF)}$-*msrD*$_{(1-3)}$:*yfp*) resulted in the elimination of the fluorescence induction (Fig. 2a), demonstrating that *msrDL* translation is an important and necessary cis-acting feature to regulate *msrD*$_{(1-3)}$:*yfp* expression as reported for *ermC*[47].

In bacteria, antibiotic-dependent gene induction relies mainly on translational or transcriptional attenuation[48]. To determine if *msrDL* prompts a transcriptional or translational attenuation, northern blots analysis with a probe located in *msrD*$_{(1-3)}$:*yfp* 3' UTR were performed on total RNA extracted from cell exposed or not to ERY and/or IPTG. A 1.2-kb band corresponding to *msrDL-msrD*$_{(1-3)}$:*yfp* mRNA is transcribed in presence of IPTG and starts to increase steadily 5 min after exposure to 100 nM ERY (Fig. 2b). Consistent with this ERY-

8

206   dependent transcript accumulation, we concluded that *msrD* regulation by *msrDL* occurs at

207   the transcription level.

208   　　　Transcription attenuation employs premature transcription termination via: (i) Rho-

209   dependent terminator (RDT) by binding of Rho factor, a RecA-type ATPase, to a C-rich and

210   G-poor sequence known as Rho utilization site[49]; (ii) Rho-independent terminator (RIT) where

211   a stable GC-rich stem-loop followed by a poly-uridine sequence causes RNAP to drop off[50].

212   Treatment with bicyclomycin, a Rho inhibitor, did not result in constitutive expression of the

213   reporter, thus excluding the possibility of RDT attenuation (Supplementary fig. 2b). Analysis of

214   the intergenic region between *msrDL* and *msrD* using ARNold server[51] revealed the presence

215   of a RIT with a ΔG of -7.9 kcal.mol^{-1}. We also identified a consensus TTNTTT NusG-dependent

216   RNAP pausing site embedded in *msrDL* sequence (Fig. 2c and Supplementary fig. 2a), as

217   previously described for *vmlR* [52,53]. In order to test this possible transcription termination

218   activity, we generated a mutant by removing the putative terminator (referred as pMMB-

219   msrDL$_{(no\_term)}$-msrD$_{(1-3)}$:*yfp*). Deletion of the terminator resulted in a constitutive expression of

220   the fluorescent reporter in absence of ERY, indicating that the terminator is a necessary cis-

221   acting regulatory feature that can terminate transcription (Fig. 2c). These results validate the

222   presence of a second transcriptional attenuator in the *mefA*/*msrD* operon that regulates

223   exclusively *msrD*.

224

225   **Selective drug-sensing by MsrDL prevents its translation elongation and termination**

226   　　　To determine how this regulation occurs via ribosome-mediated mechanism,

227   translation of *msrDL* mRNA with the PURE system[54] was subjected to various antibiotics and

228   its propensity to form SRC was analyzed by toeprinting[55] (Fig. 3 and Supplementary fig. 3). A

229   strong toeprint signal was observed in presence of ERY and AZI, while it was absent in

230   presence of TEL, TYL and SPI (Fig. 3a). This *in vitro* result is correlated to *in vivo* observations

231   made with the *msrD*$_{(1-3)}$:*yfp* reporter gene which was also only induced by ERY and AZI, but

232   not by TEL, TYL, SPI and non-macrolide antibiotics (Fig. 3b).

9

233   We further characterized the translation of *msrDL* mRNA and showed that in presence

234   of 50 µM RTP, an inhibitor of the first peptide bond formation which allows to identify ORFs

235   start codon[56], a clear toeprint occurred (Fig. 3c). This toeprint corresponds to a ribosome

236   stalled with the initiating codon in the ribosomal P site and confirms that ribosomes can initiate

237   *msrDL* translation. The toeprint observed at positions +31, +32 and +33 relative to *msrDL* 5'

238   end (Fig. 3a and 3c) in presence of ERY and AZI indicates an SRC located at the termination

239   step of MsrDL synthesis with the C-terminal methionine (M6) codon in the P site and UAA stop

240   codon in the A site. In accordance with this, reactions depleted of release factors (RF1, RF2,

241   RF3) (Fig. 3c) show the same toeprint result. Moreover, addition of puromycin led to the loss

242   of this toeprint signal, while preserving it in presence of ERY (Fig. 3c). Puromycin is an

243   aminonucleoside antibiotic mimicking A site substrate tyrosyl-tRNA and causing premature

244   chain termination. While actively translating ribosomes are sensitive to this antibiotic, stalled

245   ones tend to be refractory[15,16,20,57,58]. The resistance of MsrDL-SRC to puromycin is consistent

246   with an ERY-sensing NC that leads to PTC silencing and stalling. The stalled ribosome on

247   ORF *msrDL* covers the first half of the hairpin of the RIT and therefore prevents its formation

248   and transcription termination (Fig. 2c and Supplementary fig. 3).

249   The main dissimilarity between tested macrolides resides in the presence or absence

250   of a cladinose moiety on C3 of the macrocyclic lactone ring which appears to be critical for

251   MsrDL-SRC formation (Fig. 3a) similarly to ErmCL[20,59]. Absence of significant toeprint in

252   presence of TEL (whose C3 cladinose sugar is replaced by a keto group) suggests that *msrDL*

253   is translated efficiently without stalling. TYL and SPI differ from the other macrolides by the

254   presence of disaccharide mycaminose-mycarose in place of the C5 monosaccharide

255   desosamine. When bound to the ribosome, this extended sugar moiety protrudes into the PTC

256   of the ribosome[60]. Absence of intermediate toeprint and increase of the toeprint corresponding

257   to initiation complex in presence of these two drugs imply that these antibiotics stabilize the

258   initiation complex. Previous results[60–62] have shown that they inhibit the formation of the

259   peptide bond, our result suggests that it occurs mainly for the first peptide bond formation (Fig.

260   3a).

10

261   We submitted the sequence of MsrDL to an alanine-scanning to investigate the

262   importance of each residue and their ability to induce $msrD_{(1-3)}$:*yfp* reporter, which indirectly

263   reports the formation of an ERY-dependent SRC. The scan shows a strong reduction of

264   inducibility for all the mutated residues with the exception Y2 (Fig. 3d). Since MsrDL is a

265   hexapeptide, it is evident that most of the amino acids would have their importance to maintain

266   a conformation able to sense ERY. A complete loss of inducibility has been observed for

267   residues L3 and I4 suggesting that these two residues were directly involved in drug-sensing,

268   which was structurally confirmed and detailed in the next section. Moreover, considering that

269   MsrDL inhibits the action of both RF1/RF2 in presence of ERY, we mutated UAA stop codon

270   into RF1-specific UAG and RF2-specific UGA stop codons to investigate a putative preferential

271   inhibition as previously shown for TnaC[63]. Mutation of UAA into UAG or UGA reduces the level

272   of inducibility of the reporter gene (Supplementary fig. 2c) demonstrating the importance of the

273   stop codon. This observation is corroborated by our phylogenetic analysis which revealed a

274   large prevalence of UAA stop codon among the different *msrDL* variants (Supplementary fig.

275   2a). Most likely the UAA stop codon has been selected by evolution to maximize *msrD*

276   expression in presence of an inducer. Mutagenesis of *msrDL* sequence by synonymous

277   codons (iso-codons) as described in Methods leads to a reduction of the *yfp* expression for

278   MsrDL$_{WT-iso}$ construct, possibly due to the lack of NusG pausing site, but the regulation is mostly

279   preserved (Fig. 3d). Therefore, the amino acid composition of the peptide is responsible for

280   the ribosome stalling. Addition of an extra alanine before the stop codon in MsrDL$_{7A-iso}$

281   construct reduces the regulatory potential of the leader peptide (Fig. 3d). Toeprinting assay

282   reveals that this construct has two stalling positions: one occurs with the additional A7 codon

283   in the ribosomal A site and the second with the stop codon in the A site (Fig. 3e). Thus, MsrDL

284   peptide seems to induce efficient ribosomal stalling by preventing elongation and termination.

285   When both are uncoupled like in the MsrDL$_{7A-iso}$ construct the regulation is less efficient (Fig.

286   3d).

11

Molecular mechanism of ribosome stalling by MsrDL

To understand how MsrDL inhibits translation termination in presence of ERY, a synthetic mRNA containing a single *msrDL* copy was translated *in vitro* with purified *E. coli* DB10 ribosomes in presence of ERY as described in Supplementary fig. 4a and the resulting sample was subjected to cryo-EM. Single-particle reconstruction of MsrDL-SRC was done by refining two subclasses, one containing only P-tRNAS and one containing P- and E-tRNAs (respectively 11% and 28.1% of total particles), as described in Methods and on Supplementary fig. 4b. It resulted an initial map of 70S ribosome (EMD-13805) with an average resolution of 3.0 Å that was subjected to multibody refinement, generating reconstructions for the body and the head of the small subunit (EMD-13807 and EMD-13808) and the large subunit (EMD-13806), presenting average resolutions of 3.08, 3.3 and 2.97 Å respectively (Supplementary fig. 4b and 4c and Supplementary Table 2). The resolutions of the derived reconstructions were consistent with clear and unambiguous assignment of ribosomal proteins side chains, rRNA nucleotides and some post-transcriptional modifications (Supplementary fig. 4d to 4f). Local resolution of the codon-anticodon allowed unambiguous identification of the P-tRNA as an elongator $_{Met}$tRNA^{Met} (Supplementary fig. 4e), which is also confirmed by the presence of distinctive elements such as N^4-acetylcytidine at position 34 (ac^{4}C34) and N^6-threonylcarbamoyladenosine at position 37 (t^{6}A37) (Supplementary fig. 4e and 4f)[64,65], consistently with the toeprint results which assigned the M6 codon in the P site and UAA stop codon in the A site (Fig. 3c).

A clear density corresponding to ERY bound in its canonical position was found at the entrance of the NPET (Fig. 4a, 4b and Supplementary fig. 4d), allowing clear attribution of macrocyclic lactone ring, cladinose and desosamine sugars. A continuous density at the 3' end of P-tRNA extending within the entrance of ribosome tunnel was identified as MsrDL-NC and local resolution of ~3 Å allowed to model the peptide *de novo* (Fig. 4b and Supplementary fig. 4d). It adopts a hook-like shape with its N-terminal extremity protruding into a cavity at the entrance of the tunnel delimited by 23S rRNA nucleotides U2584, U2586, G2608 and C2610 (Fig. 4b). One noticeable feature of MsrDL interaction with the ribosome is its residue Y2 that

bulges out the base U2584 to form a π-stacking with the base G2583 (Fig. 4c and 4d) in place of U2584. This unique interaction should stabilize the peptide conformation, while it appears structurally significant, it is not strictly essential since replacement of the Y2 by an alanine reduces by less than 50% the induction of the reporter gene (Fig. 3d). In addition, this residue is substituted in some MsrDL variants (Supplementary fig. 2a). MsrDL does not show numerous significant electrostatic interactions with the ribosome since it is mostly composed of hydrophobic amino acids. It is likely stabilized by hydrophobic interactions.

Our biochemical investigations showed that MsrDL-SRC was formed due to hampered translation termination on UAA stop codon. This stop codon is recognized by both RF1 and RF2 which subsequently catalyze peptide hydrolysis via their conserved GGQ motif protruding within the PTC. Structural alignment of our model to RF1- and RF2-containing ribosome structures[66] revealed that proper accommodation of the RFs is prevented by steric clashes of the methylated glutamine and the following glycines of the GGQ motif with the residue F5 of MsrDL and 23S rRNA bases U2584 and U2585 respectively (Fig. 4e). The conformation of MsrDL peptide stabilizes the PTC in an uninduced conformation[67] which prevents the opening of the active site necessary for peptide bond formation and hydrolysis (Fig. 4f). This observation suggests that MsrDL-SRC cannot catalyze peptide bond formation, as confirmed by the toeprinting preformed on the MsrDL$_{7A\text{-iso}}$ construct (Fig. 3e). Structural alignment of MsrDL-SRC with ErmBL- and ErmCL-SRC demonstrates that 23S rRNA nucleotides U2506 and 2585 are not in the same conformation (Supplementary fig. 5a and 5b), these bases in MsrDL-SRC being in a conformation more similar to ErmDL-, SpeFL- and TnaC(R23F)-SRC (Supplementary fig. 5c to 5e)[12–16]. However, unusual position of base U2584 seems to be a unique feature of MsrDL-SRC.

MsrDL may monitor the presence of cladinose-containing drugs as our *in vivo* and *in vitro* experiments suggested. Mutation of residues L3 and I4 abolished induction of the reporter gene suggesting that they were critical for drug recognition and/or conformation of the peptide (Fig. 3d). Consistently, in our model we identified residue L3 as the closest amino acid from cladinose moiety and residue I4 as the closest from desosamine moiety (Fig. 4b and 4g).

13

343 However, similarly to ErmBL, no close contact between the nascent chain and the drug was

344 observed[13,68], residue L3 being ~3.8 Å away from cladinose sugar and residue I4 being ~3.9

345 Å away from desosamine sugar, consistently with a hydrophobic interaction between MsrDL

346 and the drug (Fig. 4g to 4i). This observation is also corroborated by previous descriptions of

347 pentapeptides conferring ERY resistance in which the presence of a leucine or isoleucine at

348 position 3 was critical for drug recognition[69,70]. Moreover, the importance of 23S rRNA residue

349 A2062 in acting as an ERY-sensor and in contributing to silence the PTC, has been

350 demonstrated for some regulatory leader peptides[71,72]. In the case of ErmCL, the critical

351 feature for macrolide-dependent stalling is the rotation of the base A2062 that forms an

352 Hoogsteen base pairing with m^2A2503[12,71,72]. The structure of MsrDL-SRC shows that residue

353 I4 restrains rotation of base A2062 (Fig. 4j). Therefore, MsrDL induces an $A2062/m^2A2503$-

354 independent ribosome stalling[72].

355 The path of MsrDL-NC within the ribosomal tunnel contrasts from all previous

356 descriptions of elongating polypeptides (Fig. 4b and 5). Indeed, ERY-sensing ErmBL, ErmCL

357 and ErmDL leader peptides[12–14] engage in the NPET and skirt around ERY, while MsrDL

358 curves before encountering the ligand then engages into a dead-end crevice at the entrance

359 of NPET (Fig. 4b and 5b). The same observation (Fig. 5c) can be made with metabolite-

360 sensing SpeFL/TnaC(R23F) leader peptides[15,16] which avoid the crevice and enter the NPET.

361 The first methionine of MsrDL-NC latches into the dead-end crevice which is delimited by 23S

362 rRNA nucleotides U2584, U2586, G2608 and C2610 (Fig. 5a to 5c). This crevice located at

363 the base of helix 93 (h93) is part of domain V of 23S rRNA and is conserved from bacteria to

364 human (mitoribosome and cytosolic ribosome) (Fig. 5d, Supplementary fig. 5f and 5g). We

365 named it proximal crevice.

366

367 **MsrD negatively regulates its own expression**

368 MsrD protein provides antibiotic resistance by rescuing ERY-stalled ribosome while

369 *msrDL* translation in presence of ERY leads to the formation of a SRC. If MsrD is also able to

370 rescue this SRC, it will repress its own expression and form a feedback loop similarly to Vga(A)

371 [73]. We tested this hypothesis using *E. coli* DB10 strains double transformed with pMMB-*msrDL*-

372 *msrD*$_{(1-3)}$:*yfp* and the compatible pBAD plasmid expressing various *msrD* variants. Strains were

373 grown in presence of ERY at 300 nM with their optical density and fluorescence monitored

374 (Fig. 6a). Strain carrying the pBAD-*Control* showed high fluorescence and low OD$_{600}$ as

375 observed in Fig. 2a, reflecting an induction of the reporter and a susceptibility to ERY. On the

376 contrary, expression of *msrD* led to higher cell growth and a strong reduction of fluorescence

377 which correspond respectively to antibiotic resistance and repression of the expression of the

378 reporter. These results support that MsrD can rescue MsrDL-SRC and therefore releases the

379 RIT repressing *msrD* transcription.

380   The strain expressing *msrD*$_{E125Q}$ has a low ERY resistance (Fig. 1e). When it is co-

381 transformed with the pMMB-*msrDL*-*msrD*$_{(1-3)}$:*yfp* plasmid, no resistance is observed, possibly

382 because the presence of the two plasmid creates some toxicity. Overall, the results show that

383 MsrD variants that lost the ability to provide antibiotic resistance (ΔPtIM, ΔLoop and ATPase

384 deficient mutants) also lost the ability to rescue MsrDL-SRC (Fig. 6a). Point mutations in the

385 Loop of the PtIM indicated some discrepancy between antibiotic resistance phenotype and

386 MsrDL-SRC rescue. All the mutants show an intermediary phenotype with less antibiotic

387 resistance and less repression of reporter compared to MsrD. The mutant MsrD$_{H244w}$ has the

388 same repression effect on the reporter than MsrD$_{H244A}$ for an equivalent OD$_{600}$ but it provides

389 more that 3 times less antibiotic resistance (Fig. 1g and 6a). The mutant MsrD$_{R241A}$ which

390 provides a resistance close to MsrD does not rescue the MsrDL-SRC as efficiently as the latter

391 one (Fig. 1g and 6a). Mutants MsrD$_{L242A}$ and MsrD$_{H244A}$ provide similar resistance, but

392 MsrD$_{H244A}$ confers a stronger repression of the reporter (Fig. 1g and 6a). Together these

393 observations demonstrate that the determinants of the dual function of MsrD in conferring

394 antibiotic resistance and rescuing MsrDL-SRC are overall similar.

395

396 **DISCUSSION**

397   We used genetic, molecular biology and structural approaches to dissect the regulation

398 of streptococcal ARE ABC-F gene *msrD*, its effect on ERY-stalled ribosomes and to provide

15

information on ARE ABC-F mechanisms of action. We characterized the *msrDL* regulatory ORF which induces ribosome stalling in presence of cladinose-containing macrolides (Fig. 3, 4 and 6b). Our structural data show that this inhibition results from the conjoint effects of: (*i*) MsrDL maintaining 23S rRNA bases U2506 and U2585 in an uninduced conformation (Fig. 4f), (*ii*) the steric occlusion by U2584, U2585 and MsrDL residue F5 that precludes the productive accommodation of RF1/RF2 (Fig. 3c and 4e). MsrDL-stalled ribosome then hampers formation of a RIT allowing transcription of *msrD* (Fig. 2c, 3a, 3c and 6b). The coupling between translation and transcription necessary for this mechanism in *Streptococci* is possibly mediated by a NusG-dependent RNAP pausing site in *msrDL* (Fig. 2c).

MsrD binds with some specificity to ERY-stalled ribosome (Fig. 1d) and then its ATPase activity drives mechanical rearrangements to rescue stalled ribosome. The ATPase mechanism that allows the rescue is still unknown for ARE ABC-Fs and all the current structures of an ARE ABC-F in complex with the ribosome were generated with an ATPase-dead mutant[1–3,5] or use of non-hydrolysable ATP analogues[7]. These structures do not capture an antibiotic stalled complex and embodies a reaction intermediate before or after antibiotic release of an ARE ABC-F trapped on the ribosome. We provide here some evidence about possible mechanisms (Fig. 6b). We show that only one active ATPase site (Site II, MsrD$_{E125Q}$) can provide some antibiotic resistance (Fig. 1e) while generating a strong toxicity for the cell independently of the antibiotic and also shows more association with 50S (Fig 1c and 1d). The mutant of Site II (MsrD$_{E434Q}$) shows a stronger toxicity (Fig. 1e) and no antibiotic resistance, effects related to less dissociation from the ribosome (Fig. 1c and 1d). Therefore, it is possible that site I is needed for complete dissociation of MsrD from the ribosome or subunits after ATP hydrolysis occurs at site II. Mutation of both sites (MsrD$_{EQ2}$) leads to the same toxicity as for inactive Site I (Fig. 1e), suggesting that having only Site II mutated induces a new MsrD conformation that inhibits more cell growth. In accordance with these results, independent E-to-Q mutations in the ARE ABC-F Vga(A), show that mutation in site I maintains an higher ATPase activity than mutation in site II[74].

16

426   We envision two putative non-exclusive scenarios that involve for the first one, a

427   disassembling of ERY-stalled ribosomes, and for the other one, a displacement of the drug

428   followed by a restart of the translation process (Fig. 6b). A key point for future studies will be

429   to explore the ATPase activity of MsrD in a stalled-ribosome context to determine how many

430   rounds of ATP hydrolysis are necessary to rescue the latter one. The dissociation model

431   requires the hydrolysis of only two ATP molecules, while antibiotic displacement may require

432   multiple hydrolysis rounds in Site II to displace the drug and to position back the elongating

433   peptide in a correct conformation in the NPET. So far, those experiments have been

434   challenging due to the low solubility of all the ARE ABC-F proteins[2,6].

435   Alongside with ErmBL, ErmCL and ErmDL, MsrDL constitutes the fourth ERY-sensing

436   NC structurally described, however some mechanisms of drug-sensing and PTC silencing

437   differ. First, similarly to ErmCL, the presence of C3 cladinose sugar is required for stalling (Fig.

438   3a and 3b) contrary to ErmBL and ErmDL that senses drugs lacking this moiety such as

439   oleandomycin, solithromycin or telithromycin[12,14,59,68]. Second, similarly to ErmBL, no close

440   contact between the drug and MsrDL was observed (Fig. 4h and 4i)[68]. Third, MsrDL is the only

441   described leader peptide that exploits inhibition of its hydrolysis by RFs to induce stalling in

442   presence of antibiotic, similarly to the metabolite sensors TnaC and SpeFL[15,16]. On the

443   contrary, ErmBL[13], ErmCL[12] and ErmDL[14] employ only elongation inhibition. Fourth, ERY-

444   dependent stalling on *msrDL* regulates downstream *msrD* via transcriptional attenuation (Fig.

445   2b and 2c) while it relies on translational attenuation for ErmBL, ErmCL and ErmDL[14,68,75].

446   Finally, MsrDL-NC conformation and path within the ribosome greatly differ from previously

447   described ligand-sensing leader peptides that elongate within the tunnel (Fig. 5b and 5c)[12–16].

448   It adopts a hook-like shape possibly due to hydrophobic interactions with the drug (Fig. 4b, 4g

449   and 4h), while its initiating methionine engages in a dead-end crevice at the NPET entrance

450   (Fig. 5). To our knowledge, this is the first description of this crevice, conserved in prokaryotes

451   and eukaryotes (Supplementary fig. 5f and 5g), as a functional site within the ribosome and

452   we propose to name it proximal crevice.

17

453   ARE ABC-F genes tend to be transcriptionally regulated as illustrated by *msrD*, *vmlR*,

454   *vgaA*, *lmo0919* and *lmrC*[52,73,76–78]. However, MsrD can regulated its own expression by creating

455   a negative feedback-loop which is not the case for VmlR[52]. The gene *msrD* forms an operon

456   with the efflux pump *mefA* (Fig. 1a) which is also regulated *via* ribosome-mediated

457   transcriptional attenuation, translational stalling occurring on *mefAL*[33]. Therefore, *msrD* is

458   under the dual-regulation of two ERY-sensing leader peptides. One explanation for this

459   redundancy may reside in the need for the bacteria to tightly regulate *msrD* because of its

460   toxicity. Expression of $msrD_{WT}$ in *E. coli* DB10 led to a 20 % growth defect compared to control

461   condition (Fig. 1e) suggesting that $msrD_{WT}$ expression has a fitness cost for the bacteria and

462   can be beneficial only in presence of antibiotic. The presence of two attenuators creates a

463   double-lock system to avoid any basal expression in absence of inducer and the negative

464   feedback-loop maintains a minimal amount of MsrD production. Thus, as long as MefA can

465   export enough antibiotic to provide resistance, *msrD* should be kept repressed. The fitness

466   cost of the expression of ARE ABC-F genes is possibly the Achilles heel of bacteria containing

467   those genes and may be exploited to fight antibiotic resistance. MsrD provides resistance to

468   ERY, AZY and TEL[23] (Table 1) but only the first two induce its expression, indicating that MsrD

469   can provide some resistance for an antibiotic which does not induce its expression. Thus,

470   MsrDL facilitates the use of MsrD by the bacteria and maintains its evolution under its control.

471

ACKNOWLEDGMENTS

AUTHOR CONTRIBUTIONS

F.O. performed the first experiments that initiated the project. C.R.F. performed most of the experiments. S.N. performed northern blotting experiments. C.R.F. prepared the cryo-EM sample. H.S. prepared cryo-EM grids and imaged them. C.A.I. and Y.H. processed cryo-EM data. C.R.F and E.C.L. reconstructed the atomic model. G.B. initiated the project and designed the research program with Y.H. C.R.F. and G.B. wrote the paper with input from all authors.

DECLARATION OF INTERESTS

The authors declare no competing interests. Requests for materials should be addressed to G.B. (boel@ibpc.fr).

19

MAIN FIGURE TITLES AND LEGENDS

Figure 1. Translation factor MsrD alleviates erythromycin effects upon translation *in vivo*. (a) Organization of the *mefA/msrD* macrolide resistance operon. In presence of ERY, ribosomes stall during translation of *mefAL* leading to transcription anti-attenuation, both *mefA* and *msrD* being then transcribed. Similar mechanism occurs during translation of *msrDL*, which regulates transcription of *msrD* only. (b) Sequence alignment of various *msr* homologs visualized with Jalview according to percentage of identity. Positions of tested mutations are highlighted in red and indicated by arrows. Main features of ABC-F proteins are indicated on the schematic. Genebank accession numbers are indicated between brackets. See also Supplementary Fig. 1b. (c and d) Polyribosomes analysis and western blotting of *E. coli* DB10 expressing a control (pBAD-*Control*), $msrD_{WT}$ (pBAD-$msrD_{WT}$), $msrD_{EQ2}$ (pBAD-$msrD_{EQ2}$), $msrD_{E125Q}$ (pBAD-$msrD_{E125Q}$) or $msrD_{E434Q}$ (pBAD-$msrD_{E434Q}$) untreated or treated for 1 h with 25 µM ERY during mid-log phase. "L" stands for total lysate. See also Supplementary fig. 1c and 1d and Methods. (e to g) Relative growth of *E. coli* DB10 expressing *msrD* variants in presence of ERY after 24 h. Optical densities were normalized relative to optical densities of *E. coli* DB10 pBAD-*Control* grown in the absence of ERY. Error bars represent mean ± s.d. for triplicate experiments. See also supplementary Table 1.

Figure 2. Erythromycin-dependent transcriptional attenuation regulates *msrD* expression. (a) ERY-dependent induction of $msrD_{(1-3)}$:*yfp*. Fluorescent reporters shown on schematics have been introduced in *E. coli* DB10 and grew in presence of 1 mM IPTG and increasing sublethal ERY concentrations during 17 h. Fluorescence has been plotted against OD_{600}, error bars for both axes represent mean ± s.d. for triplicate experiments. (b) Northern analysis of *msrD* transcript. RNAs were extracted before adding or not 1 mM IPTG ($T_{0'}$), 10 min after adding IPTG ($T_{10'}$), and 5, 15, 30, 60, 120 min after adding or not 100 nM ERY. Location of probe in $msrD_{(1-3)}$:*yfp* 3' UTR is shown on the schematic. The presence of a second band was also observed but we hypothesized that it was abortive transcript resulting from the construct insofar as its presence correlates with induction by IPTG and ERY, and is no longer detectable using other probes (data not shown). Note the presence of leaky transcription in absence of IPTG, that is slightly amplified in presence of ERY. (c) Deletion of the intrinsic terminator between *msrDL* and $msrD_{(1-3)}$:*yfp* leads to a constitutive induction in absence of ERY. Error bars for both axes represent mean ± s.d. for triplicate experiments.

Figure 3. MsrDL is a macrolide-sensing nascent chain that stalls the ribosome. (a) Toeprinting assay of *msrDL* in the absence (-) or in the presence of 50 µM of various macrolide antibiotics. White arrow indicates initiation codon. Black arrows indicate ribosome stalling, with M6 codon in the P site. Chemical structure of antibiotics is shown, C3 cladinose sugar of ERY

20

and AZI being highlighted. See also Supplementary fig. 3. (b) *In vivo* induction of *msrD*(1:3):*yfp* by various PTC/NPET targeting antibiotics. Bacteria containing pMMB-*msrDL*-*msrD*(1:3):*yfp* were grown during 17 h in presence of 1 mM IPTG, in the absence (grey histograms) or in the presence of 50 nM antibiotics (red histograms). Error bars represent mean ± s.d. for triplicate experiments. (c) Toeprinting assay depleted of release factors was performed in the absence of ribosome (line 1), in presence of 50 μM RTP to assess start codon (line 2), without or with 50 μM ERY (line 3 and 4), without or with 50 μM ERY then supplemented with 100 μM puromycin (line 5 and 6), without or with 50 μM ERY in presence of RF1/RF2/RF3 (line 7 and 8). The schematic indicates position of toeprint signal on the synthetic mRNA, P site codon of MsrDL-SRC is underlined. See also Supplementary fig. 3. (d) Effects of *msrDL* variants on the expression of *msrD*(1:3):*yfp*. Bacteria were grown during 17 h in presence of 1 mM IPTG, in the absence (grey histograms) or in the presence of 100 nM ERY (red histograms). Error bars represent mean ± s.d. for triplicate experiments, square boxes show fold of induction. (e) Toeprinting assay performed on the MsrDL$_{7A\text{-iso}}$ construct in absence or presence of ERY. Addition of a sense codon after M6 codon leads to translational arrest with M6 codon in the P site (grey arrows) and A7 codon in the A site in presence of ERY. A faint toeprint is also observed with A7 codon in the P site (black arrows) and the stop codon in the A site.

Figure 4. Structure of MsrDL-SRC. (a) Transverse section of the cryo-EM map showing the 30S (grey) and 50S (white) ribosomal subunits, mRNA (purple), ERY (red) and MsrDL-NC (gold) bound to P-site tRNA^{Met} (beige). (b) Close-up of MsrDL-NC within ribosomal tunnel showing experimental density and modelled structure, colored as Fig. 4A while 23S rRNA nucleotides are shown in light grey. (c and d) Presence of MsrDL residue Y2 displace nucleotide U2584 out of its position when compared to RF1- (PDB 5J30, light blue) and RF2-containing (PDB 5CZP, blue) termination complex, thus forming a π-stacking with G2583 [66]. (e) Conformation of U2584 and U2585 prevent productive accommodation of RF1 (PDB 5J30, light blue) and RF2 (PDB 5CZP, blue) while catalytic methylated glutamine would clash with MsrDL residue F5[66]. (f) PTC in MsrDL-SRC (light grey) is stabilized in an uninduced state (PDB 1VQ6, pink) rather than in an induced state (PDB 1VQN, green) as U2585 is pushed back by MsrDL residue Y2[67]. (g to i) Molecular basis for C3 cladinose sugar recognition by MsrDL. Residue L3 is at proximity of cladinose sugar while residue I4 is at proximity of desosamine sugar. TEL lacking cladinose sugar and failing to form MsrDL-SRC has been aligned (PDB 4V7S) [79]. (j) Presence of residue I4 avoids rotation of A2062 to form an Hoogsteen base pairing with m^{2}A2503 as it is the case for ErmCL-SRC (PDB 3J7Z, green)[12]. Light blue dashed lines indicate hydrogen bonds formed by Hoogsteen base pairing. For the whole figure, structures were aligned on domain V of 23S rRNA. Spheres represent van der Waals radii.

21

Figure 5. MsrDL engages in a conserved crevice at the NPET entrance. (a) Secondary structure of the *E. coli* 23S rRNA domain V showing location of the proximal crevice at the base of h93. For the whole figure, nucleotides delimitating proximal crevice are shown in red. (b and c) Comparison of MsrDL path (gold) with ERY-dependent leader peptides ErmBL (PDB 5JTE, blue), ErmCL (PDB 3J7Z, green), ErmDL (PDB 7NSO, teal) as well as L-ornithine-sensing SpeFL (PDB 6TC3, pink) and L-tryptophan-sensing TnaC(R23F) (PDB 7O1A, purple)[12–16]. See also Supplementary fig. 5a to 5e. (d) Proximal crevice in domain V is conserved from bacteria to human (MsrDL-SRC, grey; *S. aureus* PDB 6YEF, light green; *H. sapiens* 55S mitoribosome PDB 7A5F, light blue; *H. sapiens* 80S ribosome PDB 6OLI, marine blue)[80–82]. See also Supplementary fig. 5g and 5h. For the whole figure, atomic model of MsrDL is shown with its experimental density. Structures were aligned on domain V of 23S rRNA.

Figure 6. MsrD negatively regulates its own synthesis upon erythromycin exposure. (a) Effects of MsrD variants on MsrDL. *E. coli* DB10 containing pMMB-*msrDL-msrD*(1-3):*yfp* and expressing various *msrD* mutants were grown in presence of 0.2 % L-Arabinose, 1 mM IPTG and 300 nM ERY, both OD_{600} and fluorescence being recorded over 24 h. Fluorescence has been plotted against OD_{600}, error bars for both axes represent mean ± s.d. for triplicate experiments. Color code is same as Fig. 1e to 1g. Light green rectangle indicates bacterial growth over control plasmid. (b) Model of MsrD regulating its own expression and providing antibiotic resistance. Presence of a NusG-dependent pause site may stall the RNAP and provides explanation why the system works in bacteria where transcription and translation are not so tightly coupled. In absence of ERY, RNAP drops off at Rho-independent transcription terminator. In presence of ERY, the ribosome following the RNAP (presumably paused) stalls and unwinds the terminator leading to *msrD* transcription. Once translated, MsrD negatively regulates its own expression on one side, and provides antibiotic resistance on the other side. ATP-bound MsrD recognizes ERY-stalled ribosome and may either expel the antibiotic or dissociate the ribosome, ATP site II being active. Activity in ATP site I may lead to MsrD dissociation and recycling.

MAIN TABLE TITLES AND LEGENDS

Table 1. Minimum inhibitory concentration (MIC) and half maximal inhibitory concentration (IC$_{50}$) of *E. coli* DB10 expressing *msrD* in presence of ribosome-targeting antibiotics. See Methods for experimental details.

	pBAD-*Control*		pBAD-*msrD*$_{WT}$	
Antibiotic	**MIC (μM)**	**IC$_{50}$ (μM)**	**MIC (μM)**	**IC$_{50}$ (μM)**
Erythromycin	2	0,179 ± 0,007	16	4,592 ± 0,582
Azithromycin	0.25	0,046 ± 0,002	2	0,953 ± 0,053
Telithromycin	1	0,086 ± 0,008	2	0,714 ± 0,066
Tylosin	4	1,649 ± 0,151	4	1,672 ± 0,103
Spiramycin	2	0,758 ± 0,063	2	0,81 ± 0,078
Lincomycin	32	12,61 ± 2,154	32	12,62 ± 1,27
Linezolid	32	13,62 ± 2,064	32	13,41 ± 1,137
Retapamulin	1	0,071 ± 0,004	1	0,075 ± 0,007

23

METHOD DETAILS

Construction of plasmids

Strains and plasmids used in this study are listed in Supplementary Table 3. Oligonucleotides are listed in Supplementary Table 4. For the whole study, the considered reference sequence for *mefA/msrD* macrolide resistance operon was a Tn916-type transposon inserted in *Streptococcus pneumoniae* strain 23771 genome (Genbank accession number FR671415.1)[83]. Plasmids pBAD-*Control* and pBAD-*msrD*$_{WT}$ containing a C-terminal hexahistidine tag (originally referred as pBAD33 and pVN50) were kindly retrieved from Olivier Chesneau at Institut Pasteur (Paris, France)[24]. Both *mefA/msrD* macrolide resistance operon and pBAD-*msrD*$_{WT}$ encode the same protein MsrD (Uniprot accession number A0A496M710).

pBAD plasmids. Those plasmids allow a tight and stringent expression control via catabolite repression, interest gene being repressed in presence of 0.4 % (w/v) β-D-Glucose and induced in presence of 0.2 % (w/v) L-Arabinose. Transformed clones were selected with 20 µg.ml^{-1} chloramphenicol. In this study, all *msrD* mutants contain a C-terminal hexahistidine tag. Catalytic mutant *msrD*$_{EQ2}$ was generated by amplifying pBAD-*msrD*$_{WT}$ with primer pairs 5/6 and 7/8, both fragments being assembled with NEBuilder HiFi DNA Assembly Master Mix (New England Biolabs). Catalytic mutants *msrD*$_{E125Q}$, *msrD*$_{E434Q}$ were generated via quickchange mutagenesis with primers pairs 9/10 and 11/12. Mutants *msrD*$_{\Delta Loop}$ and *msrD*$_{\Delta PtIM}$ were generated based on phylogenetic alignments by deleting residues between K216/K254 and E189/A274 respectively, a three-glycine linker being added to allow flexibility, via quickchange mutagenesis using primer pairs 13/14 and 15/16. Variants *msrD*$_{R241A}$, *msrD*$_{L242A}$, *msrD*$_{H244A}$, *msrD*$_{H244W}$ were generated via fusion PCR by amplifying *msrD*$_{WT}$ with primers pairs 1/18, 1/20, 1/22, 1/24 and 2/17, 2/19, 2/21, 2/23 respectively. Backbone was amplified with primer pair 3/4 and fragments were assembled with NEBuilder HiFi DNA Assembly Master Mix (New England Biolabs).

pMMB plasmids. All pMMB constructs originated from a low copy IPTG-inducible plasmid pMMB67EH-*yfp*, consisting in original pMMB67EH[45] containing optimized *venus-yfp* enhancing its translation under the control of P$_{tac}$ promoter (manuscript in preparation). Transformed clones were selected with 100 µg.ml^{-1} ampicillin. To test *msrDL* functions *in vivo*, several fluorescent reporter genes have been designed. First, pMMB67EH-*yfp* native P$_{tac}$ promoter was replaced by P$_{LlacO-1}$ promoter as previously described[46]:

5'- ATAAATGTGAGCGGATAACATTGACATTGTGAGCGGATAACAAGATACTGAGCAC**A** - 3' (lac operators, shaded grey; transcription start, bold). This IPTG-inducible promoter allows a tight and stringent transcription regulation compared to P$_{tac}$ promoter, insofar as no regulatory element is found in the 5' UTR. Promoter was replaced by amplifying pMMB67EH-*yfp* with primer pairs 25/26, PCR fragment being then re-circularized via NEBuilder HiFi DNA Assembly

24

Master Mix (New England Biolabs). The resulting plasmid was named pMMBpLlacO-1-67EH-*yfp*. Plasmid pMMB-*msrDL*-*msrD*(1–3):*yfp* has been designed by introducing the sequence spanning from the first nucleotide downstream *mefA* stop codon to *msrD* three first codons fused to *yfp*. The introduced sequence is as follows: 5'-ACAATATT**GGAGGA**ATATTT ATGTATCTTATTTTCATGTAA CTCTTCCTGCTAAAATCGCAGGGTTTTCCCTGCATACAAGCAAATGAAAGCATGCGATTATAGACA**GGAGGA**AATGTT<u>A TGGAATTA</u>-3' (RBS, bold; *msrDL*, shaded grey, *msrD* three first codons are underlined). To clone such construct, *yfp* gene was amplified from pMMB67EH-*yfp* with primer pairs 27/29 then with 28/29 to generate the insert, backbone was amplified with primer pair 30/31 using pMMBpLlacO-1-67EH-*yfp* as matrix, both fragments being then assembled with NEBuilder HiFi DNA Assembly Master Mix (New England Biolabs). Plasmid pMMB-*control* was built by removing the *msrDL*-*msrD*(1–3):*yfp* cassette via quickchange mutagenesis using primer pair 32/33, the resulting construction containing only the P$_{LlacO-1}$ promoter followed by the plasmid endogenous *rrnB* transcription terminator. Plasmid pMMB-*msrDL*(no_term)-*msrD*(1–3):*yfp* (where the RIT between *msrDL* and *msrD* is deleted) was generated by amplifying pMMB-*msrDL*-*msrD*(1–3):*yfp* with primer pair 34/35, PCR fragment being then re-circularized via NEBuilder HiFi DNA Assembly Master Mix (New England Biolabs). The various *msrDL* mutants were cloned via quickchange mutagenesis by amplifying pMMB-*msrDL*-*msrD*(1–3):*yfp* with primers 36 to 51. Plasmid pMMB-*msrDL*(MYLIFMA-isocodons)-*msrD*(1–3):*yfp* was generated by replacing *msrDL*$_{WT}$ sequence (ATGTATCTTATTTTCATGTAA) by a recoded sequence (ATGTACCTGATCTTCATGGCCTAA) using isocodons and introducing an extra alanine codon (7A codon) before stop codon. Sequence was recoded using isocodons because mutating the WT sequence introduced a new promoter. To do so, pMMB-*msrDL*-*msrD*(1–3):*yfp* was amplified with primer pair 52/53, PCR fragment being then re-circularized via NEBuilder HiFi DNA Assembly Master Mix (New England Biolabs). Recoded sequence without the 7A codon (ATGTACCTGATCTTCATGTAA) was generated via quickchange mutagenesis by amplifying pMMB-*msrDL*(MYLIFMA-isocodons)-*msrD*(1–3):*yfp* with primer pair 54/55, leading to plasmid pMMB-*msrDL*(WT-isocodons)-*msrD*(1–3):*yfp*.

Antibiotic susceptibility testing, MIC and IC50 determination

A saturated preculture of *E. coli* DB10 transformed with pBAD plasmid was grown overnight at 37 °C under vigorous shaking in Luria-Bertani Miller broth (LB), 20 µg.ml^{-1} chloramphenicol and supplemented with 0.4 % (w/v) β-D-Glucose. Antibiotic susceptibility testing assay was performed in Mueller-Hinton broth (MH, Sigma Aldrich), antibiotics being diluted via serial dilutions. A 96-wells flat-bottom plate (Flacon) was filled with a final volume per well of 200 µl, containing 20 µg.ml^{-1} chloramphenicol and 0.2 % (w/v) L-Arabinose and antibiotic to test. Wells were inoculated at OD$_{600}$ ~0.03-0.04 prior to addition of 60 µl mineral oil (Sigma Aldrich)

25

680   avoiding evaporation but not oxygen diffusion. Plates were therefore incubated for 24 h in

681   CLARIOstar Plus plate reader (BMG Labtech) at 37 °C with 600 rpm double-orbital shaking,

682   OD_{600} being measured each 30 min. Optical densities at 24 h were then normalized relative to

683   optical densities of *E. coli* DB10 pBAD-*Control* grown in the absence of antibiotic in Prism

684   7(GraphPad). MIC was determined as absence of growth compared to blank, IC50 was

685   calculated   in   Prism   using   equation   Y=Bottom + (Top-

686   Bottom)/(1 + ((X^HillSlope)/(IC50^HillSlope))) and the standard deviation was calculated by

687   multiplying standard error by square root of n (n being at least 3 replicates). To generate

688   curves, for bacteria grown in absence of antibiotic (0 µM), since coordinates are plotted as

689   logarithms and since log(0) is undefined, this point has been approximated 2 log units below

690   the lowest tested value (*i.e.* 0.0625 µM) consistently with Prism user guide[84]. Curve fitting was

691   performed with non-linear fitting function "log(inhibitor) vs. response -- Variable slope" using

692   Y=Bottom + (Top-Bottom)/(1+10^((LogIC50-X)*HillSlope)). Both equations gave strictly the

693   same result for IC_{50}.

694

695   *In vivo* **induction assay**

696   A saturated preculture of *E. coli* DB10 transformed with pMMB plasmid was grown overnight

697   at 37 °C under vigorous shaking in LB with 100 µg.ml^{-1} ampicillin. For bacteria double-

698   transformed with pMMB and pBAD plasmids, media was also supplemented with 20 µg.ml^{-1}

699   chloramphenicol and supplemented with 0.4 % (w/v) β-D-Glucose. *In vivo* induction assay was

700   performed in Mueller-Hinton broth (MH, Sigma Aldrich). A 96-wells flat-bottom plate (Flacon)

701   was filled with a final volume per well of 200 µl, containing 100 µg.ml^{-1} ampicillin, 1 mM

702   Isopropyl β-D-1-thiogalactopyranoside (IPTG). Growth medium was supplemented with 20

703   µg.ml^{-1} chloramphenicol and 0.2 % (w/v) L-Arabinose if pBAD plasmid is present. Induction of

704   fluorescent reporters being antibiotic-dependent, growth media were supplemented with

705   required antibiotic accordingly. Plates were therefore incubated in CLARIOstar Plus plate

706   reader (BMG labtech) at 37 °C with 600 rpm double-orbital shaking up to 24 h, OD_{600} and

707   fluorescence (excitation: 497-15 nm, emission: 540-20 nm, gain 1600) being measured each

708   30 min.

709

710   **Polyribosomes fractionation**

711   Saturated precultures of *E. coli* DB10 transformed with pBAD-*control*, pBAD-*msrD*$_{WT}$, pBAD-

712   *msrD*$_{EQ2}$, pBAD-*msrD*$_{E125Q}$ or pBAD-*msrD*$_{E434Q}$ were grown overnight at 37 °C under vigorous

713   shaking in LB, 20 µg.ml^{-1} chloramphenicol, 0.4 % (w/v) β-D-Glucose. Growth media (MH, 20

714   µg.ml^{-1} chloramphenicol, 0.2 % (w/v) L-Arabinose) was inoculated at OD_{600}=0.05 with

715   normalized precultures, and cells were grown at 37 °C and 180 rpm. When OD_{600}=0.5 was

716   reached, cultures were divided in two and one half was treated with a 25 µM erythromycin.

26

717 Cultures were then incubated 1 hour at 37 °C and 180 rpm before harvesting. Cultures were

718 chilled and cells were harvested by centrifuging 10 min at 8 000 rpm, 4 °C. Supernatant was

719 discarded and cells were resuspended in 350 µl of lysis buffer (20 mM Tris pH 8, 20 mM MgCl$_2$,

720 100 mM NH$_4$(OAc), 2 mM β-mercaptoethanol, 1 mg.ml^{-1} lysozyme) and transferred in

721 microtubes. Then, 30 µl of sodium deoxycholate 10 % (w/v) was added and cells were

722 mechanically lysed by 3 rounds of freezing-thawing. Lysates were clarified by centrifuging 20

723 min at 18 000 xg, 4 °C and total RNAs were quantified. Finally, 500 µg of total RNAs were

724 loaded onto 10-40 % (w/v) sucrose gradients (20 mM Tris pH 8, 20 mM MgCl$_2$, 100 mM

725 NH$_4$(OAc), 2 mM β-mercaptoethanol) and centrifuged 2 h at 40 000 rpm, 4 °C in SW41 rotor

726 (Beckman Coulter). Samples were fractionated and collected using Biocomp Piston Gradient

727 Fractionator (BioComp Instruments), absorbance being measured at 254 nm.

728

729 **Immunoblotting**

730 Fractions of 400 µl were precipitated in ice-cold absolute ethanol (1 volume of sample, 3

731 volumes of ethanol) overnight at -20 °C. Samples were then centrifuged 45 min at 18 000 xg,

732 4 °C. Supernatant was removed and samples were vacuum-dried. Pellets were resuspended

733 in 33.3 µl 1X Laemmli buffer, 10 µl being loaded on 12.5 % acrylamide SDS-PAGE gels.

734 Concerning total lysates, 10 µg of normalized total RNAs were loaded as control. Gels were

735 resolved by migrating at 0.04 A and then applied on Immun-Blot PVDF membrane (Bio-Rad)

736 that had been activated in absolute ethanol then washed in electro-transfer buffer (25 mM Tris

737 base, 192 mM glycine, 0.1 % (w/v) SDS, 10 % (v/v) absolute ethanol). Proteins were electro-

738 transferred at 100 V during 1 h. Membranes were blocked by incubating 1 h in 1X PBS

739 supplemented with 0.5 % nonfat dry milk then washed with 1X PBS. C-term His-tagged MsrD$_{WT}$

740 and MsrD$_{EQ2}$ were detected using anti-6xHis-tag primary antibody (Covalab, 1:2 000 dilution

741 in 1X PBS, 0.1 % Tween-20) combined with anti-mouse-HRP secondary antibody (Covalab,

742 1:20 000 dilution in 1X PBS, 0.1 % Tween-20). Immunoblots were revealed by performing an

743 ECL detection using Clarity Western ECL Substrate (Bio-Rad) and imaged with Li-Cor

744 Odyssey FC imaging system (Li-Cor).

745

746 **Preparation of *E. coli* DB10 ribosomes**

747 An overnight saturated *E. coli* DB10 preculture was used to inoculate growth medium (LB,

748 dilution 1:100) and cells were grown at 37 °C and 180 rpm. When OD$_{600}$=0.5, cells were

749 washed and harvested by two centrifugations during 20 min, 5 000 xg at 4°C followed by

750 resuspensions in Buffer A (20 mM Tris pH 7.4, 10 mM Mg(OAc), 100 mM NH$_4$(OAc), 0.5 mM

751 EDTA). Pellets were resuspended in Buffer A supplemented with 6 mM β-mercaptoethanol,

752 10 mg.ml^{-1} lysozyme, 0.001 % (v/v) protease inhibitor cocktail (Sigma Aldrich) and lysed three

753 times at 2.5 kBar using a cell disrupter (Constant Systems Limited). Lysate was clarified by

27

two centrifugations during 15 min, 22 000 xg at 4°C then spun for 20 h, 34 700 rpm at 4 °C in a Type 70 Ti rotor (Beckmann Coulter) through a 37.7 % (w/v) sucrose cushion in Buffer B (20 mM Tris pH 7.4, 10 mM Mg(OAc), 500 mM NH_4(OAc), 0.5 mM EDTA, 6 mM β-mercaptoethanol). Sucrose cushions were decanted and ribosome pellets resuspended in Buffer C (20 mM Tris pH 7.4, 7.5 mM Mg(OAc), 60 mM NH_4(OAc), 0.5 mM EDTA, 6 mM β-mercaptoethanol). Finally, 12 mg of ribosomes were loaded onto 10-40 % (w/v) sucrose gradients in Buffer C and centrifuged 18 h at 20 000 rpm, 4 °C in SW28 rotor (Beckman Coulter). Gradients were fractionated using Biocomp Piston Gradient Fractionator (BioComp Instruments), absorbance being measured at 254 nm. Fractions containing 70S ribosomes were pooled, washed and concentrated in Amicon 50k (Merckmillipore) using Buffer C. Ribosomes concentration was adjusted to 18-20 µM, then aliquoted and flash frozen in liquid nitrogen.

RNA extraction and northern blotting

Total RNA extraction was realized using the RNAsnap method as previously described[85]. In brief, a preculture of *E. coli* DB10 containing pMMB-*msrDL-msrD*$_{(1–3)}$:*yfp* was grown overnight at 37 °C under vigorous shaking in LB supplemented with 100 µg.ml^{-1} ampicillin. Growth medium (MH, 100 µg.ml^{-1} ampicillin) was inoculated at OD_{600}=0.05, and cells were grown at 37 °C and 180 rpm. When OD_{600}=0.5, cells were treated (or not) with 1 mM IPTG during 10 min, then treated (or not) with 100 nM erythromycin. Samples of 2 ml were collected ($T_{0'}$ = before IPTG was added, $T_{10'}$= 10 min after IPTG was added, and 5 min, 15 min, 30 min, 60 min and 120 min after erythromycin was added), then spun during 1 min at 15 000 rpm. Growth media was removed and cells were resuspended in 100 µl RNAsnap buffer (95 % (v/v) formamide, 18 mM EDTA, 0.025 % (v/v) SDS, 1 % (v/v) β-mercaptoethanol). Samples were heated for 10 min at 95 °C then clarified by centrifuging 10 min, at 16 000 rpm at 16 °C. For northern blotting analysis, 6 µg of total RNAs were resolved on a 1 % (w/v) agarose gel then transferred onto Amersham Hybond-N+ Membrane (GE Healthcare) by capillary transfer. Radioactive probe was prepared using 40 pmol of primer 59 and 5'-labelled with 10 U of T4 Polynucleotide Kinase (New England Biolabs) and [γ^{32}P]ATP (150 µCi). Probe was hybridized overnight at 42 °C using ULTRAhyb-Oligo hybridization buffer (Thermo Fisher Scientific). Membrane was washed three times at 42 °C during 15 min (once in 2x SSC + 0.1 % (v/v) SDS, once in 1x SSC + 0.1 % (v/v) SDS and finally in 0.1x SSC + 0.1 % (v/v) SDS). Radioactive signal was visualized by exposing 4 h a Storage Phosphor Screen BAS-IP MS 2040 (Fujifilm) then imaged with a Typhoon FLA 9500 (GE Healthcare).

In vitro transcription

In vitro transcription was carried out in T7 RiboMAX Large Scale RNA Production System kit (Promega) according to manufacturer instructions. Briefly, to generate DNA matrix (Supplementary Table 5), T7 promoter (5'-GCGAATTAATACGACTCACTATAGGG-3') was added by PCR using primers pair 56/57 (Supplementary Table 4) and pMMB plasmids as templates. Transcription reactions were incubated 4 h at 37 °C and transcripts were purified with TRIzol Reagent (Thermo Fisher Scientific) and Direct-zol RNA Miniprep kit (Zymo Research), samples being eluted in THE Ambion RNA Storage Solution (Thermo Fisher Scientific). Final concentration was adjusted to 5 pmol.µl^{-1}.

Toeprinting assay

Position of stalled ribosomes on mRNA was determined by toeprinting assay, slightly adapted from previously described methods[15,86]. *In vitro* translation reactions were performed using PURExpress ΔRF123 kit and PURExpress ΔRibosome (New England Biolabs) according to manufacturer instructions. Briefly, prior to *in vitro* translation reactions, 0.5 µl of 500 µM ligand (e.g. erythromycin etc) was dried in a micro-centrifuge tube, using a SpeedVac vacuum concentrator (Thermo Fisher Scientific), final concentration being 50 µM once resuspended in a 5 µl reaction. Reactions were incubated during 15 min at 37 °C using 5 pmol of RNA templates (generated as described above) and 3.3 µM of purified *E. coli* DB10 ribosomes. When needed, samples were treated with 100 µM final puromycin and incubated 3 min more. Immediately, 2 pmol of CY5-labelled primer 58 complementary to NV1 sequence [20] was added and incubated for 5 min at 37 °C. For each reaction, reverse transcription was performed with 0.5 µl (corresponding to 5 U) of Avian Myeloblastosis Virus Reverse Transcriptase (Promega), 0.1 µl dNTP mix (10 mM), 0.4 µl Pure System Buffer (5 mM K-phosphate pH 7.3, 9 mM Mg(OAc), 95 mM K-glutamate, 5 mM NH$_4$Cl, 0.5 mM CaCl$_2$, 1 mM spermidine, 8 mM putrescine, 1 mM DTT) and incubated 20 min at 37 °C. Reactions were quenched with 1 µl NaOH 5 M and incubated 15 min at 37 °C. Alkali were therefore neutralized by adding 0.7 µl HCl 25% immediately supplemented with 20 µl toe-printing resuspension buffer (300 mM Na(OAc) pH 5.5, 5 mM EDTA, 0.5% (v/v) SDS). Finally, cDNAs were purified using QIAquick Nucleotide Removal kit (Qiagen), vacuum dried and resuspended in 6 µl formamide dye (95% (v/v) formamide, 20 mM EDTA, 0.25% (w/v) bromophenol blue). Sanger sequencing was performed on DNA matrix used for *in vitro* transcription. Briefly, each 20 µl reaction contained 7.5 nM DNA matrix, 75 nM CY5-labelled primer 58, 40 µM of each dNTPs, 0.025 U Taq Pol (New England Biolabds), 1x Thermo Pol Buffer (New England Biolabs) and corresponding ddNTPs (625 µM ddCTP/ddTTP/ddATP or 50 µM ddGTP). After PCR, 20 µl formamide dye was added to each sequencing reaction. Samples were denatured 3 min at 80 °C, then 5 µl of

825 sequencing reaction and 1.5 µl of toe-printing reaction were loaded on a 6% acrylamide/bis-
826 acrylamide (19:1) sequencing gel containing 8 M urea. Gel was resolved by migrating 90 min
827 at 50 W, then imaged using a Typhoon FLA 9500 (GE Healthcare Life Sciences) using CY5
828 mode, LPR Ch.2 filter and 635 nm laser.

829

830 **Preparation of MsrDL-SRC**

831 A DNA matrix (Supplementary Table 5) was prepared with CloneAmp HiFi PCR Premix
832 (Takara) using primer pair 56/60 (Supplementary Table 4) and plasmid pMMB-*msrDL*-
833 *msrD*$_{(1-3)}$:*yfp* as matrix. The corresponding mRNA was generated as described above. The
834 complete sequence of MsrDL-SRC mRNA is:

835 5'- GGAGCGGAUAACAAGAUACUGAGCACAACAAUAUU**GGAGG**AAUAUUUAUGUAU
836 CUUAUUUUCAUGUAACUCUUCCUGCUAAAAUCGCAGGGUUUUCCUGC -3' (RBS, bold;
837 *msrDL*, shaded grey; the ATG codon in the P site of stalled ribosomes is underlined). Prior to
838 *in vitro* translation reaction, 1 µl of 500 µM erythromycin (50 µM final concentration once
839 resuspended in 10 µl) has been dried in a micro-centrifuge tube, using a SpeedVac vacuum
840 concentrator (Thermo Fisher Scientific). Dried erythromycin has been resuspended in a 10 µl
841 *in vitro* translation reaction carried out in PURE*frex* 2.0 kit (Genefrontier), containing 1.83 µM
842 of purified *E. coli* DB10 ribosomes and 3.6 µM mRNA (molar ratio 1:2). The reaction has been
843 incubated for 10 minutes at 37 °C, before adding 100 µM final puromycin, and incubated 3 min
844 more. Reaction was therefore diluted in ribosome purification Buffer C (20 mM Tris pH 7.4, 7.5
845 mM Mg(OAc), 60 mM NH$_4$(OAc), 0.5 mM EDTA, 6 mM β-mercaptoethanol) to reach a
846 concentration of 150 nM ribosomes. Cryo-EM grids were immediately prepared.

847

848 **Cryo-EM grids preparation**

849 Safematic ccu-010 HV carbon coater was used to coat Quantifoil carbon grids (QF-R2/2-Cu)
850 with a thin carbon layer of approximate thickness of 2nm. Grids were therefore glow discharged
851 for 30 sec at 2 mA. Then, 4 µl of *in vitro* translation reaction diluted to 150 nM were applied,
852 and after a 2 sec blotting (force 5) and 30 sec waiting time, grids were vitrified in liquid ethane
853 using a Vitrobot Mark IV (FEI) set to 4 °C and 100 % humidity.

854

855 **Image acquisition and processing**

856 Data collection was performed on a Talos Arctica instrument (FEI Company) at 200 kV using
857 the EPU software (Thermo Fisher Company) for automated data acquisition. Data were
858 collected at a nominal defocus of -0.5 to -2.7 µm at a magnification of 120,000 X yielding a
859 calibrated pixel size of 1.2 Å. Micrographs were recorded as movie stack on a K2 Summit
860 direct electron detector (Gatan), each movie stack were fractionated into 65 frames for a total

861 exposure of 6.5 sec corresponding to an electron dose of 64 e⁻/Å². MotionCor2 [87] was used for

862 dose weighting, drift and whole-frame motion correction. A dose weighted average image of

863 the whole stack was used to determine the contrast transfer function with the software Gctf[88].

864 Particles were picked using a Laplacian of gaussian function (min diameter 260 Å, max

865 diameter 320 Å). A total of ~254k particles were extracted from a subset of motion-corrected

866 images (1523 micrographs) presenting a resolution equal or better than 4 Å with a box size of

867 360 pixels. The particles were binned three folds for 2D and subsequent 3D classification. After

868 2 rounds of 2D classification in RELION 3[89], ~158k particles were selected and submitted to

869 Relion 3D classification[89]. A class of non-rotated 70S depicting high-resolution features and

870 bearing a tRNA with various occupancies was selected, representing ~104k particles. This

871 class was further 3D-classified with a spherical mask engulfing the tRNAs binding sites

872 (Supplementary Fig. 4b) into 4 classes, thus yielding to P- and E-tRNAs, P-tRNAs only, A- and

873 P-tRNAs and E-tRNAs 70S reconstructions. Only P- and E-tRNAs and P-tRNAs only

874 reconstructions were used for further processing, which represents ~62k particles displaying

875 the same global conformation of the 70S. These particles where re-extracted at the full pixel

876 size (1.2 Å) and refined through the 3D auto-refinement performed in RELION 3[89] resulting in

877 a 3 Å reconstruction (Supplementary Fig. 4c), after CTF-refinement, Bayesian particle

878 polishing and post-processing in RELION 3. In spite of the sufficient local resolution at the

879 vicinity of MsrDL peptide at the PTC (~3Å), residual movements of the 30S around the 50S

880 can be deduced by the lower local resolutions of the head and the body of the 30S. In order to

881 improve their resolution so to derive a complete atomic model of the entire 70S complex, we

882 applied RELION 3 multi-body refinement by defining three bodies; 50S, 30S-head and 30S-

883 body. After completion of the refinement, the reconstructions of the 30S-head, 30S-body and

884 50S reached average resolutions of 3.3, 3.08 and 2.97 Å, respectively. The local resolution

885 (Supplementary Fig. 4b and 4d) was estimated using ResMap[90].

886

Model building and refinement

888 The atomic model of erythromycin-stalled *Escherichia coli* 70S ribosome with streptococcal

889 MsrDL nascent chain was built into cryo-EM maps using Coot and Phenix[91,92]. Insofar as *E.*

890 *coli* DB10 hasn't been sequenced yet, we assumed that ribosomal proteins and rRNAs were

891 strictly identical to *E. coli* K12. Furthermore, we did not notice any significant features in the

892 map. Structure of SpeFL-SRC in response to L-ornithine was used as initial model (PDB

893 6TC3)[15] and has been fitted in 70S ribosome map EMD-13805. Then, each part of the

894 ribosome (50S, 30S Body and 30S Head) has been individually inspected in the corresponding

895 map (respectively EMD-13806, EMD-13807 and EMD-13808) modified if necessary in Coot.

896 P-site elongator tRNA $_{Met}$tRNA^{Met} was modeled *de novo* based on *E. coli* K12 MG1655 *metT*

897 gene, posttranscriptional modifications were added consistently with Modomics database[93]

31

898 (http://genesilico.pl/modomics/). E-site tRNA $_{Phe}$tRNA^{Phe} was derived from crystal structure of

899 phenylalanine tRNA from *E. coli* (PDB 6Y3G) with minor adjustments[94]. ERY, MsrDL leader

900 peptide and mRNA were modeled *de novo* in Coot. Final model was refined in map EMD-

901 13805 using Phenix[92].

902

Figure preparation

904 Growth curves, histograms and polyribosomes profiles were generated using GraphPad Prism

905 7 (GraphPad). Sequence alignments were visualized with JalView[95]. Western blotting, northern

906 blotting and toe-printing gels were analyzed using Fiji[96]. Figures depicting molecular structures

907 or electronic density maps were prepared using PyMOL Molecular Graphics System, Chimera

908 and ChimeraX[97,98].

909

Quantification and statistical analysis

911 Statistical details can be found in the figure legends. Statistical significance was assessed

912 using unpaired t-Test function in Prism 7 (GraphPad).

913

Data and software availability

915 Cryo-EM map of erythromycin-stalled *Escherichia coli* 70S ribosome with streptococcal MsrDL

916 nascent chain has been deposited at the Electron Microscopy Data Bank (EMDB) with

917 accession code EMD-13805, as well as 50S, 30S Body and 30S Head maps obtained after

918 multibody refinement with accession code EMD-13806, EMD-13807, EMD-13808 respectively.

919 Corresponding atomic model has been deposited in the Protein Data Bank (PDB) with

920 accession code 7Q4K.

921

REFERENCES

1. Crowe-McAuliffe, C. *et al.* Structural basis for antibiotic resistance mediated by the Bacillus subtilis ABCF ATPase VmlR. *PNAS* **115**, 8978–8983 (2018).

2. Crowe-McAuliffe, C. *et al.* Structural basis of ABCF-mediated resistance to pleuromutilin, lincosamide, and streptogramin A antibiotics in Gram-positive pathogens. *Nat Commun* **12**, 3577 (2021).

3. Crowe-McAuliffe, C. *et al.* Structural basis for PoxtA-mediated resistance to phenicol and oxazolidinone antibiotics. *Nat Commun* **13**, 1860 (2022).

4. Lenart, J., Vimberg, V., Vesela, L., Janata, J. & Balikova Novotna, G. Detailed Mutational Analysis of Vga(A) Interdomain Linker: Implication for Antibiotic Resistance Specificity and Mechanism. *Antimicrob Agents Chemother* **59**, 1360–1364 (2015).

5. Mohamad, M. *et al.* Sal-type ABC-F proteins: intrinsic and common mediators of pleuromutilin resistance by target protection in staphylococci. *Nucleic Acids Research* **50**, 2128–2142 (2022).

6. Sharkey, L. K. R., Edwards, T. A. & O'Neill, A. J. ABC-F Proteins Mediate Antibiotic Resistance through Ribosomal Protection. *mBio* **7**, (2016).

7. Su, W. *et al.* Ribosome protection by antibiotic resistance ATP-binding cassette protein. *PNAS* **115**, 5157–5162 (2018).

8. Boël, G. *et al.* The ABC-F protein EttA gates ribosome entry into the translation elongation cycle. *Nat Struct Mol Biol* **21**, 143–151 (2014).

9. Chen, B. *et al.* EttA regulates translation by binding the ribosomal E site and restricting ribosome-tRNA dynamics. *Nat Struct Mol Biol* **21**, 152–159 (2014).

10. Fostier, C. R. *et al.* ABC-F translation factors: from antibiotic resistance to immune response. *FEBS Letters* **595**, 675–706 (2021).

11. Ousalem, F., Singh, S., Chesneau, O., Hunt, J. F. & Boël, G. ABC-F proteins in mRNA translation and antibiotic resistance. *Research in Microbiology* **170**, 435–447 (2019).

12. Arenz, S. *et al.* Drug Sensing by the Ribosome Induces Translational Arrest via Active Site Perturbation. *Molecular Cell* **56**, 446–452 (2014).

13. Arenz, S. *et al.* A combined cryo-EM and molecular dynamics approach reveals the mechanism of ErmBL-mediated translation arrest. *Nat Commun* **7**, (2016).

14. Beckert, B. *et al.* Structural and mechanistic basis for translation inhibition by macrolide and ketolide antibiotics. *Nat Commun* **12**, 4466 (2021).

15. Herrero del Valle, A. *et al.* Ornithine capture by a translating ribosome controls bacterial polyamine synthesis. *Nature Microbiology* **5**, 554–561 (2020).

16. van der Stel, A.-X. *et al.* Structural basis for the tryptophan sensitivity of TnaC-mediated ribosome stalling. *Nat Commun* **12**, 5340 (2021).

17. Horinouchi, S. & Weisblum, B. Posttranscriptional modification of mRNA conformation: Mechanism that regulates erythromycin-induced resistance. *PNAS* **77**, 7079–7083 (1980).

18. Ito, K. & Chiba, S. Arrest Peptides: Cis-Acting Modulators of Translation. *Annu. Rev. Biochem.* **82**, 171–202 (2013).

19. Narayanan, C. S. & Dubnau, D. Evidence for the translational attenuation model: ribosome-binding studies and structural analysis with an in vitro run-off transcript of ermC. *Nucleic Acids Res* **13**, 7307–7326 (1985).

20. Vazquez-Laslop, N., Thum, C. & Mankin, A. S. Molecular Mechanism of Drug-Dependent Ribosome Stalling. *Molecular Cell* **30**, 190–202 (2008).

33

21. Gay, K. & Stephens, D. S. Structure and Dissemination of a Chromosomal Insertion Element Encoding Macrolide Efflux in Streptococcus pneumoniae. *The Journal of Infectious Diseases* **184**, 56–65 (2001).

22. Roberts, M. C. *et al.* Nomenclature for Macrolide and Macrolide-Lincosamide-Streptogramin B Resistance Determinants. *Antimicrob Agents Chemother* **43**, 2823–2830 (1999).

23. Daly, M. M., Doktor, S., Flamm, R. & Shortridge, D. Characterization and Prevalence of MefA, MefE, and the Associated msr(D) Gene in Streptococcus pneumoniae Clinical Isolates. *J Clin Microbiol* **42**, 3570–3574 (2004).

24. Nunez-Samudio, V. & Chesneau, O. Functional interplay between the ATP binding cassette Msr(D) protein and the membrane facilitator superfamily Mef(E) transporter for macrolide resistance in Escherichia coli. *Research in Microbiology* **164**, 226–235 (2013).

25. Tatsuno, I. *et al.* Functional Predominance of msr(D), Which Is More Effective as mef(A)-Associated Than mef(E)-Associated, Over mef(A)/mef(E) in Macrolide Resistance in Streptococcus pyogenes. *Microbial Drug Resistance* **24**, 1089–1097 (2018).

26. Zhang, Y. *et al.* Predominant role of msr(D) over mef(A) in macrolide resistance in Streptococcus pyogenes. *Microbiology (Reading)* **162**, 46–52 (2016).

27. Del Grosso, M., Camilli, R., Iannelli, F., Pozzi, G. & Pantosti, A. The mef(E)-Carrying Genetic Element (mega) of Streptococcus pneumoniae: Insertion Sites and Association with Other Genetic Elements. *Antimicrob Agents Chemother* **50**, 3361–3366 (2006).

28. Del Grosso, M., Scotto d'Abusco, A., Iannelli, F., Pozzi, G. & Pantosti, A. Tn2009, a Tn916-Like Element Containing mef(E) in Streptococcus pneumoniae. *Antimicrob Agents Chemother* **48**, 2037–2042 (2004).

29. Chancey, S. T. *et al.* Composite mobile genetic elements disseminating macrolide resistance in Streptococcus pneumoniae. *Front. Microbiol.* **6**, (2015).

30. Iannelli, F. *et al.* Nucleotide sequence of conjugative prophage Φ1207.3 (formerly Tn1207.3) carrying the mef(A)/msr(D) genes for efflux resistance to macrolides in Streptococcus pyogenes. *Front Microbiol* **5**, (2014).

31. González-Zorn, B. *et al.* Genetic basis for dissemination of armA. *Journal of Antimicrobial Chemotherapy* **56**, 583–585 (2005).

32. Ambrose, K. D., Nisbet, R. & Stephens, D. S. Macrolide Efflux in Streptococcus pneumoniae Is Mediated by a Dual Efflux Pump (mel and mef) and Is Erythromycin Inducible. *Antimicrob Agents Chemother* **49**, 4203–4209 (2005).

33. Chancey, S. T. *et al.* Transcriptional Attenuation Controls Macrolide Inducible Efflux and Resistance in Streptococcus pneumoniae and in Other Gram-Positive Bacteria Containing mef/mel(msr(D)) Elements. *PLOS ONE* **10**, e0116254 (2015).

34. Ramu, H., Mankin, A. & Vazquez-Laslop, N. Programmed drug-dependent ribosome stalling. *Mol Microbiol* **71**, 811–824 (2009).

35. Sothiselvam, S. *et al.* Macrolide antibiotics allosterically predispose the ribosome for translation arrest. *Proc Natl Acad Sci U S A* **111**, 9804–9809 (2014).

36. de Block, T. *et al.* WGS of Commensal Neisseria Reveals Acquisition of a New Ribosomal Protection Protein (MsrD) as a Possible Explanation for High Level Azithromycin Resistance in Belgium. *Pathogens* **10**, 384 (2021).

37. Lu, C. *et al.* Phenotypic and Genetic Characteristics of Macrolide and Lincosamide Resistant Ureaplasma urealyticum Isolated in Guangzhou, China. *Curr Microbiol* **61**, 44–49 (2010).

38. Sharma, P. *et al.* Comparison of Antimicrobial Resistance and Pan-Genome of Clinical and Non-Clinical Enterococcus cecorum from Poultry Using Whole-Genome Sequencing. *Foods* **9**, 686 (2020).

39. Nikaido, H. Multidrug Resistance in Bacteria. *Annual Review of Biochemistry* **78**, 119–146 (2009).

40. Nikaido, H. & Pagès, J.-M. Broad-specificity efflux pumps and their role in multidrug resistance of Gram-negative bacteria. *FEMS Microbiol Rev* **36**, 340–363 (2012).

41. Datta, N., Hedges, R. W., Becker, D. & Davies, J. Plasmid-determined Fusidic Acid Resistance in the Enterobacteriaceae. *Microbiology,* **83**, 191–196 (1974).

42. Kannan, K. *et al.* The general mode of translation inhibition by macrolide antibiotics. *Proc Natl Acad Sci U S A* **111**, 15958–15963 (2014).

43. Vázquez-Laslop, N. & Mankin, A. S. How macrolide antibiotics work. *Trends Biochem Sci* **43**, 668–684 (2018).

44. Murina, V. *et al.* ABCF ATPases Involved in Protein Synthesis, Ribosome Assembly and Antibiotic Resistance: Structural and Functional Diversification across the Tree of Life. *Journal of Molecular Biology* **431**, 3568–3590 (2019).

45. Fürste, J. P. *et al.* Molecular cloning of the plasmid RP4 primase region in a multi-host-range tacP expression vector. *Gene* **48**, 119–131 (1986).

46. Lutz, R. & Bujard, H. Independent and Tight Regulation of Transcriptional Units in Escherichia Coli Via the LacR/O, the TetR/O and AraC/I1-I2 Regulatory Elements. *Nucleic Acids Res* **25**, 1203–1210 (1997).

47. Dubnau, D. Induction of ermC requires translation of the leader peptide. *EMBO J* **4**, 533–537 (1985).

48. Dersch, P., Khan, M. A., Mühlen, S. & Görke, B. Roles of Regulatory RNAs for Antibiotic Resistance in Bacteria and Their Potential Value as Novel Drug Targets. *Front. Microbiol.* **8**, (2017).

49. Banerjee, S., Chalissery, J., Bandey, I. & Sen, R. Rho-dependent Transcription Termination: More Questions than Answers. *J Microbiol* **44**, 11–22 (2006).

50. Ray-Soni, A., Bellecourt, M. J. & Landick, R. Mechanisms of Bacterial Transcription Termination: All Good Things Must End. *Annual Review of Biochemistry* **85**, 319–347 (2016).

51. Naville, M., Ghuillot-Gaudeffroy, A., Marchais, A. & Gautheret, D. ARNold: A web tool for the prediction of Rho-independent transcription terminators. *RNA Biology* **8**, 11–13 (2011).

52. Takada, H. *et al.* Expression of Bacillus subtilis ABCF antibiotic resistance factor VmlR is regulated by RNA polymerase pausing, transcription attenuation, translation attenuation and (p)ppGpp. *Nucleic Acids Res* gkac497 (2022) doi:10.1093/nar/gkac497.

53. Yakhnin, A. V. *et al.* NusG controls transcription pausing and RNA polymerase translocation throughout the Bacillus subtilis genome. *Proc Natl Acad Sci U S A* **117**, 21628–21636 (2020).

54. Shimizu, Y. *et al.* Cell-free translation reconstituted with purified components. *Nat Biotechnol* **19**, 751–755 (2001).

55. Hartz, D., McPheeters, D. S., Traut, R. & Gold, L. Extension inhibition analysis of translation initiation complexes. in *Methods in Enzymology* vol. 164 419–425 (Academic Press, 1988).

56. Meydan, S. *et al.* Retapamulin-Assisted Ribosome Profiling Reveals the Alternative Bacterial Proteome. *Molecular Cell* **74**, 481-493.e6 (2019).
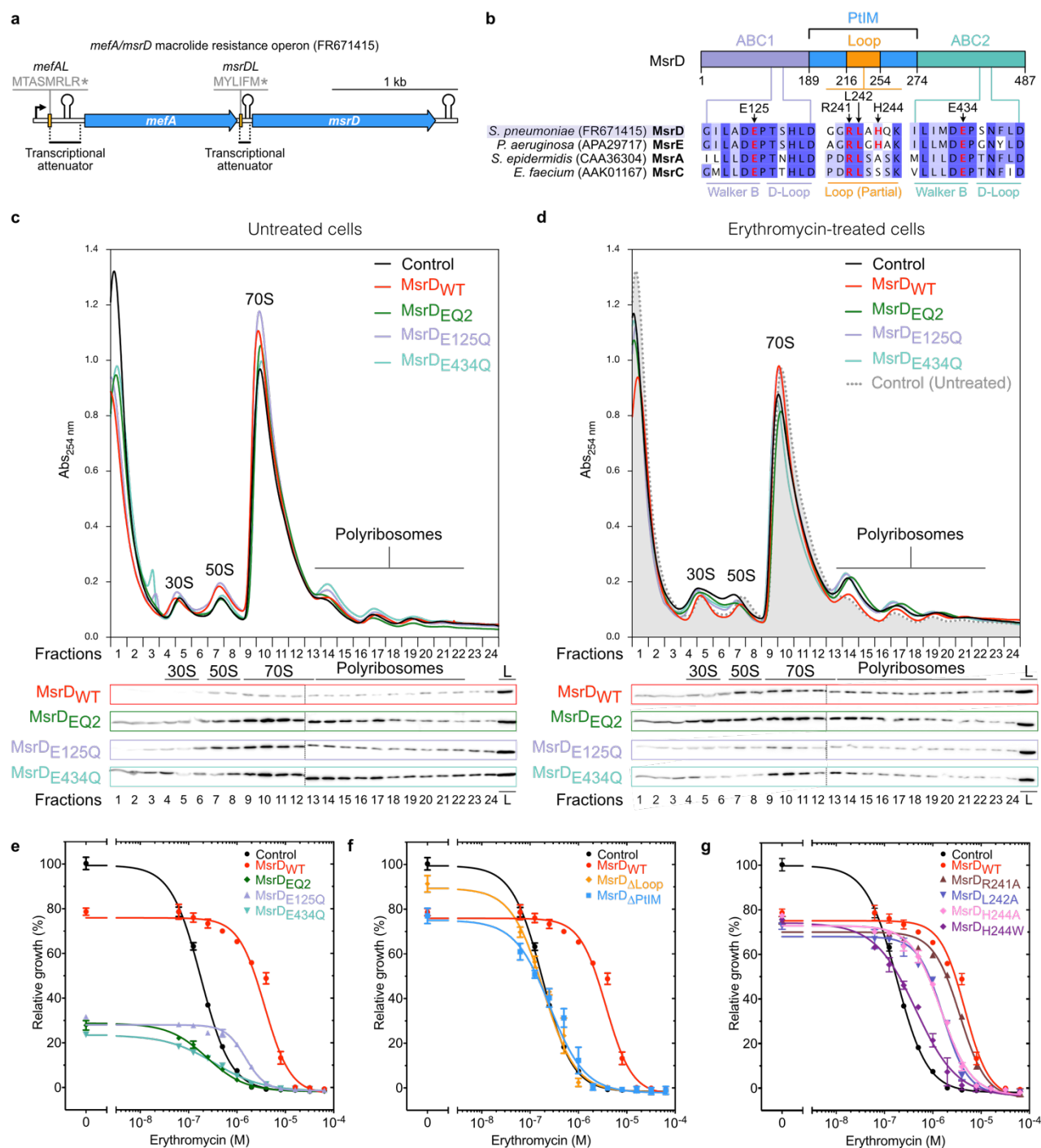
57. Muto, H., Nakatogawa, H. & Ito, K. Genetically Encoded but Nonpolypeptide Prolyl-tRNA Functions in the A Site for SecM-Mediated Ribosomal Stall. *Molecular Cell* **22**, 545–552 (2006).

58. Seip, B. & Innis, C. A. How Widespread is Metabolite Sensing by Ribosome-Arresting Nascent Peptides? *Journal of Molecular Biology* **428**, 2217–2227 (2016).

59. Vázquez-Laslop, N. *et al.* Role of antibiotic ligand in nascent peptide-dependent ribosome stalling. *Proc. Natl. Acad. Sci. U.S.A.* **108**, 10496–10501 (2011).

60. Hansen, J. L. *et al.* The Structures of Four Macrolide Antibiotics Bound to the Large Ribosomal Subunit. *Molecular Cell* **10**, 117–128 (2002).

61. Mao, J. C. & Robishaw, E. E. Effects of macrolides on peptide-bond formation and translocation. *Biochemistry* **10**, 2054–2061 (1971).

62. Poulsen, S. M., Kofoed, C. & Vester, B. Inhibition of the ribosomal peptidyl transferase reaction by the mycarose moiety of the antibiotics carbomycin, spiramycin and tylosin1 1Edited by D. E. Draper. *Journal of Molecular Biology* **304**, 471–481 (2000).

63. Emmanuel, J. S., Sengupta, A., Gordon, E. R., Noble, J. T. & Cruz-Vera, L. R. The regulatory TnaC nascent peptide preferentially inhibits release factor 2-mediated hydrolysis of peptidyl-tRNA. *J Biol Chem* **294**, 19224–19235 (2019).

64. Ohashi, Z. *et al.* Characterization of C+ located in the first position of the anticodon of Escherichia coli tRNAMet as N4-acetylcytidine. *Biochimica et Biophysica Acta (BBA) - Nucleic Acids and Protein Synthesis* **262**, 209–213 (1972).

65. Varshney, U., Lee, C. P. & RajBhandary, U. L. From elongator tRNA to initiator tRNA. *PNAS* **90**, 2305–2309 (1993).

66. Pierson, W. E. *et al.* Uniformity of Peptide Release Is Maintained by Methylation of Release Factors. *Cell Reports* **17**, 11–18 (2016).

67. Schmeing, T. M., Huang, K. S., Strobel, S. A. & Steitz, T. A. An induced-fit mechanism to promote peptide bond formation and exclude hydrolysis of peptidyl-tRNA. *Nature* **438**, 520–524 (2005).

68. Arenz, S. *et al.* Molecular basis for erythromycin-dependent ribosome stalling during translation of the ErmBL leader peptide. *Nature Communications* **5**, 3501 (2014).

69. Lovmar, M. *et al.* The Molecular Mechanism of Peptide-mediated Erythromycin Resistance *. *Journal of Biological Chemistry* **281**, 6742–6750 (2006).

70. Tenson, T., Xiong, L., Kloss, P. & Mankin, A. S. Erythromycin Resistance Peptides Selected from Random Peptide Libraries*. *Journal of Biological Chemistry* **272**, 17425–17430 (1997).

71. Koch, M., Willi, J., Pradère, U., Hall, J. & Polacek, N. Critical 23S rRNA interactions for macrolide-dependent ribosome stalling on the ErmCL nascent peptide chain. *Nucleic Acids Res* **45**, 6717–6728 (2017).

72. Vázquez-Laslop, N., Ramu, H., Klepacki, D., Kannan, K. & Mankin, A. S. The key function of a conserved and modified rRNA residue in the ribosomal response to the nascent peptide. *EMBO J* **29**, 3108–3117 (2010).

73. Vimberg, V. *et al.* Ribosome-Mediated Attenuation of vga(A) Expression Is Shaped by the Antibiotic Resistance Specificity of Vga(A) Protein Variants. *Antimicrobial Agents and Chemotherapy* **64**, (2020).

74. Jacquet, E. *et al.* ATP Hydrolysis and Pristinamycin IIA Inhibition of the Staphylococcus aureus Vga(A), a Dual ABC Protein Involved in Streptogramin A Resistance *. *Journal of Biological Chemistry* **283**, 25332–25339 (2008).

75. Mayford, M. & Weisblum, B. Conformational alterations in the ermC transcript in vivo during induction. *EMBO J* **8**, 4307–4314 (1989).

76. Dar, D. *et al.* Term-seq reveals abundant ribo-regulation of antibiotics resistance in bacteria. *Science* **352**, aad9822 (2016).

77. Koberska, M. *et al.* Beyond Self-Resistance: ABCF ATPase LmrC Is a Signal-Transducing Component of an Antibiotic-Driven Signaling Cascade Accelerating the Onset of Lincomycin Biosynthesis. *mBio* **12**, e0173121 (2021).

78. Ohki, R., Tateno, K., Takizawa, T., Aiso, T. & Murata, M. Transcriptional Termination Control of a Novel ABC Transporter Gene Involved in Antibiotic Resistance in Bacillus subtilis. *J Bacteriol* **187**, 5946–5954 (2005).

79. Dunkle, J. A., Xiong, L., Mankin, A. S. & Cate, J. H. D. Structures of the Escherichia coli ribosome with antibiotics bound near the peptidyl transferase center explain spectra of drug action. *Proc Natl Acad Sci U S A* **107**, 17152–17157 (2010).

80. Desai, N. *et al.* Elongational stalling activates mitoribosome-associated quality control. *Science* **370**, 1105–1110 (2020).

81. Golubev, A. *et al.* Cryo-EM structure of the ribosome functional complex of the human pathogen Staphylococcus aureus at 3.2 Å resolution. *FEBS Letters* **594**, 3551–3567 (2020).

82. Li, W. *et al.* Structural basis for selective stalling of human ribosome nascent chain complexes by a drug-like molecule. *Nat Struct Mol Biol* **26**, 501–509 (2019).

83. Croucher, N. J. *et al.* Rapid pneumococcal evolution in response to clinical interventions. *Science* **331**, 430–434 (2011).

84. Miller, J. R. *GraphPad Prism Version 4.0 Step-by-Step Examples*. vol. GraphPad Software Inc., San Diego (GraphPad Software Inc., San Diego, 2003).

85. Stead, M. B. *et al.* RNAsnap™: a rapid, quantitative and inexpensive, method for isolating total RNA from bacteria. *Nucleic Acids Res* **40**, e156 (2012).

86. Seefeldt, A. C. *et al.* The proline-rich antimicrobial peptide Onc112 inhibits translation by blocking and destabilizing the initiation complex. *Nature Structural & Molecular Biology* **22**, 470–475 (2015).

87. Zheng, S. Q. *et al.* MotionCor2 - anisotropic correction of beam-induced motion for improved cryo-electron microscopy. *Nat Methods* **14**, 331–332 (2017).

88. Zhang, K. Gctf: Real-time CTF determination and correction. *J Struct Biol* **193**, 1–12 (2016).

89. Zivanov, J. *et al.* New tools for automated high-resolution cryo-EM structure determination in RELION-3. *eLife* **7**, e42166 (2018).

90. Kucukelbir, A., Sigworth, F. J. & Tagare, H. D. The Local Resolution of Cryo-EM Density Maps. *Nat Methods* **11**, 63–65 (2014).

91. Emsley, P. & Cowtan, K. Coot: model-building tools for molecular graphics. *Acta Cryst D* **60**, 2126–2132 (2004).

92. Liebschner, D. *et al.* Macromolecular structure determination using X-rays, neutrons and electrons: recent developments in Phenix. *Acta Cryst D* **75**, 861–877 (2019).

93. Boccaletto, P. *et al.* MODOMICS: a database of RNA modification pathways. 2017 update. *Nucleic Acids Res* **46**, D303–D307 (2018).

94. Bourgeois, G. *et al.* Structural basis of the interaction between cyclodipeptide synthases and aminoacylated tRNA substrates. *RNA* **26**, 1589–1602 (2020).

95. Waterhouse, A. M., Procter, J. B., Martin, D. M. A., Clamp, M. & Barton, G. J. Jalview Version 2—a multiple sequence alignment editor and analysis workbench. *Bioinformatics* **25**, 1189–1191 (2009).

96. Schindelin, J. *et al.* Fiji: an open-source platform for biological-image analysis. *Nature Methods* **9**, 676–682 (2012).

97. Goddard, T. D. *et al.* UCSF ChimeraX: Meeting modern challenges in visualization and analysis. *Protein Sci* **27**, 14–25 (2018).

98. Pettersen, E. F. *et al.* UCSF Chimera—A visualization system for exploratory research and analysis. *Journal of Computational Chemistry* **25**, 1605–1612 (2004).

1171

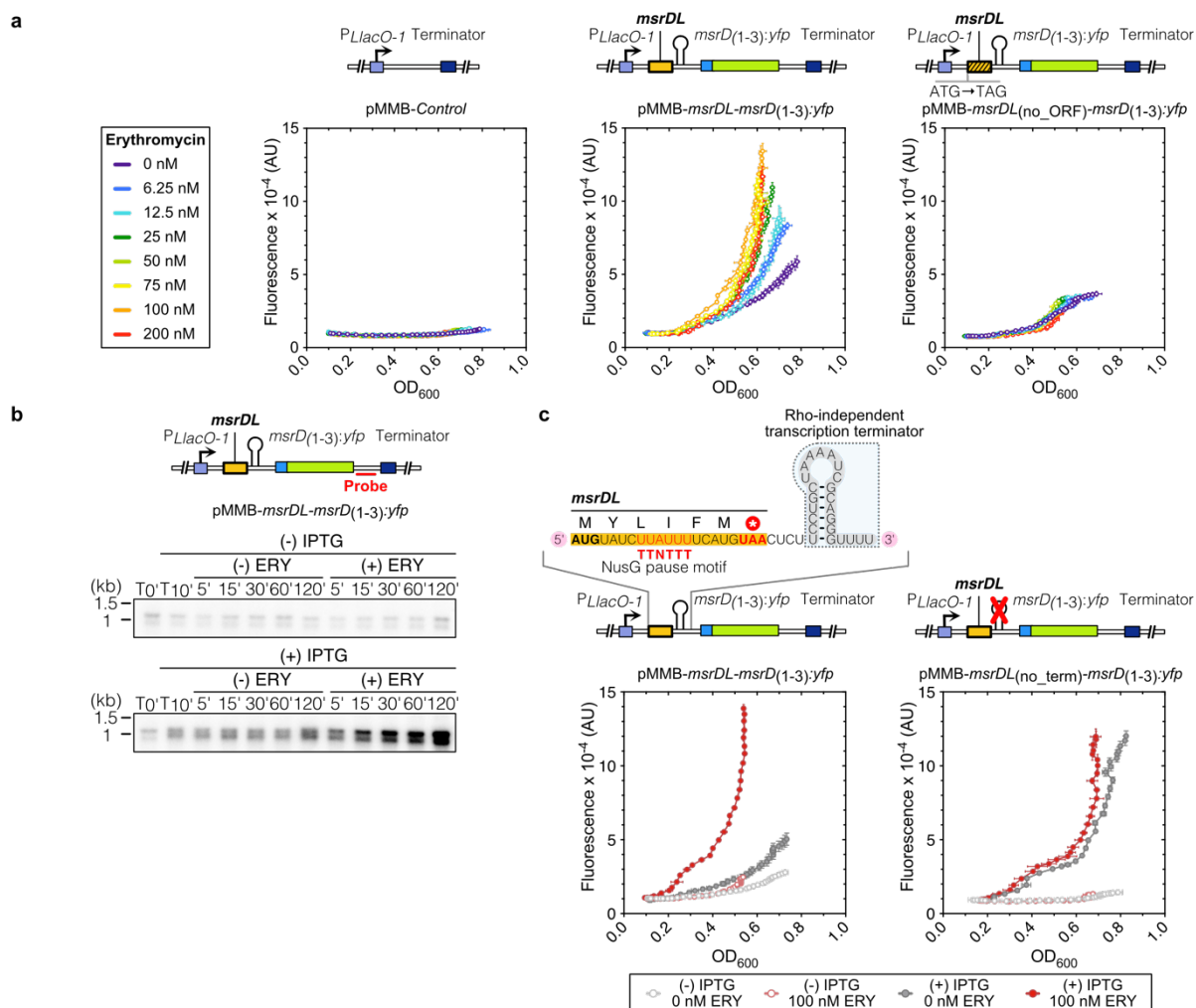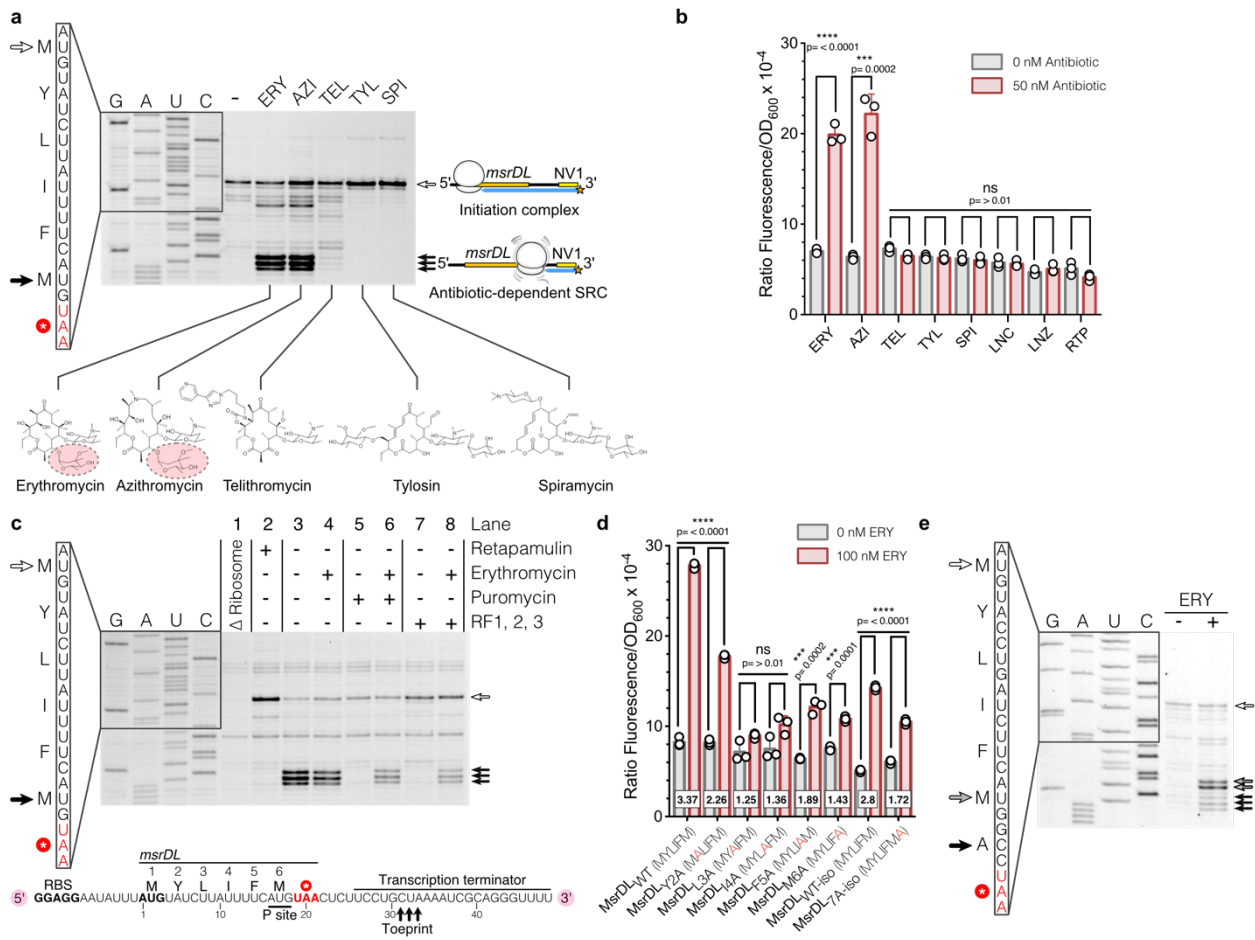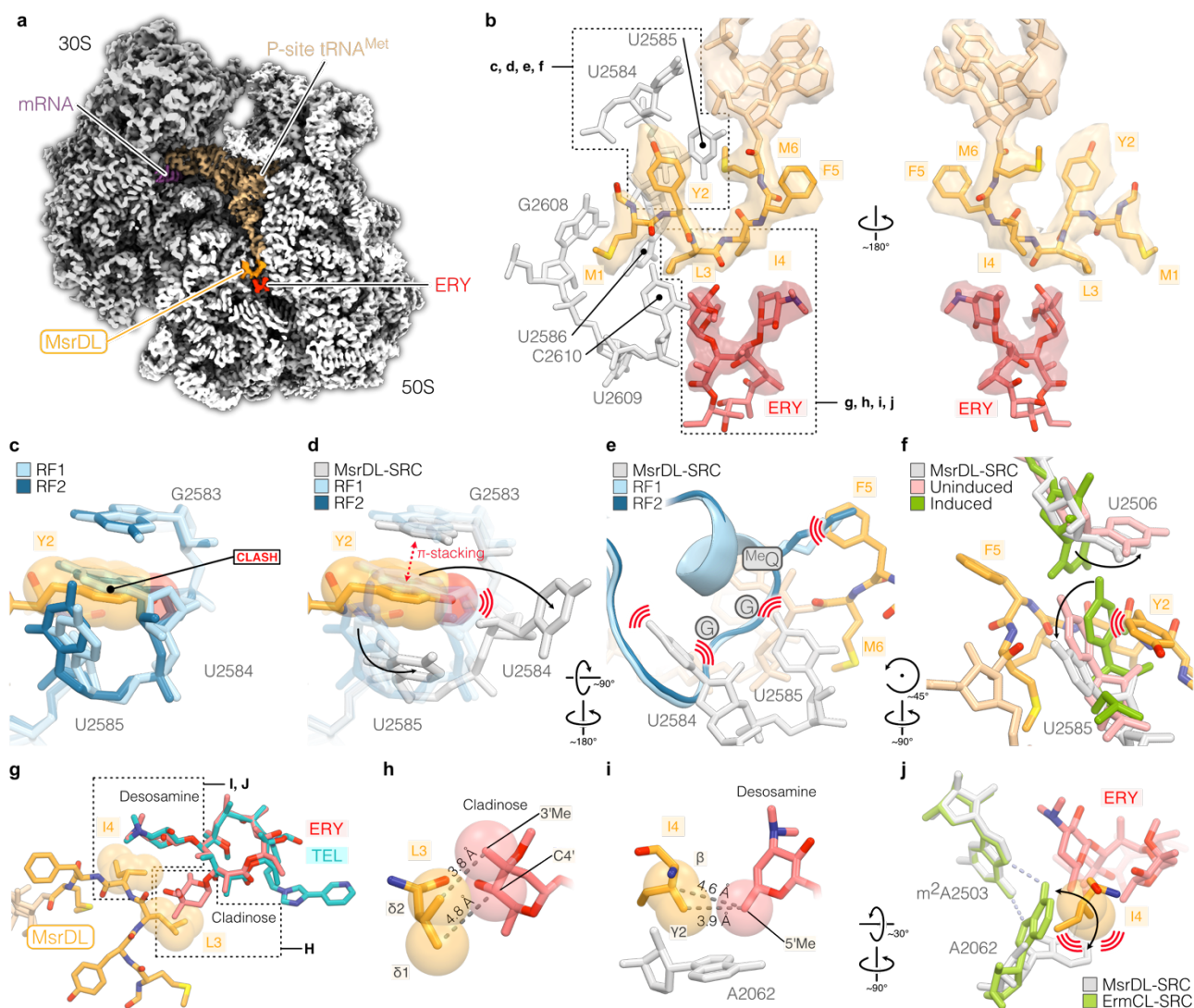# FIGURE 1

39

1172

FIGURE 2

40
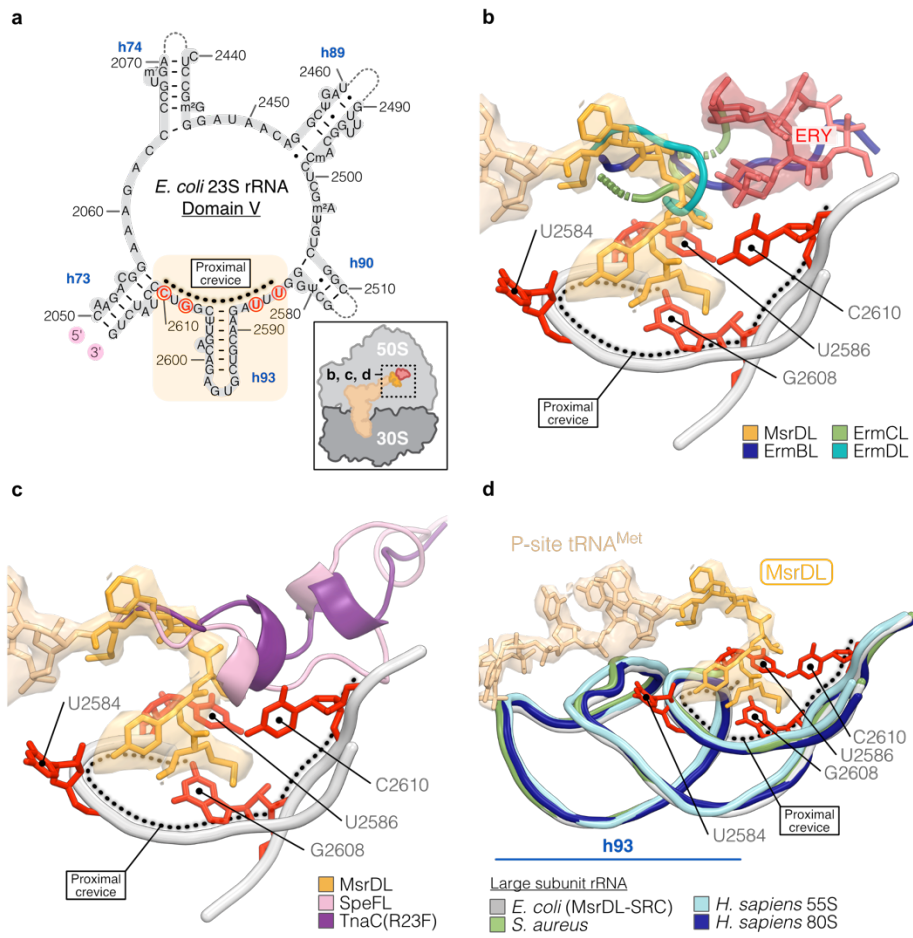
1173

FIGURE 3

1174

FIGURE 4

42

FIGURE 5

1176

FIGURE 6